Montclair State University

Montclair State University Digital Commons

Theses, Dissertations and Culminating Projects

5-2010

Conformational Motion Associated with Catalysis in Indole-3-Glycerol Phosphate Synthase from S. Solfataricus

Tomasz Kurcon

Follow this and additional works at: https://digitalcommons.montclair.edu/etd

Part of the Biochemistry Commons, and the Chemistry Commons

Abstract

Indole-3-glycerol phosphate synthase from *Sulfolobus solfataricus* (SsIGPS) belongs to a broad family of $(\beta\alpha)_8$-barrel enzymes. It catalyzes the fifth step in tryptophan biosynthesis, converting 1-(o-carboxylphenylamino)-1-deoxyribulose-5-phosphate (CdRP) to indole-3-glycerol phosphate (IGP). Site selective mutagenesis was used to introduce a single cysteine in two loops near the active site, generating two recombinant proteins, each containing a single cysteine handle. The two construct were labeled, each with two different thiol-reactive probes generating four labeled constructs that were used for this study. Steady-state kinetic parameters of the labeled mutants and the wild type SsIGPS were well characterized using fluorescence spectroscopy. Subsequent experiments under single turnover (STO) conditions were employed. In the STO experiments stopped-flow instrument was used to observe IGP accumulation and change in emission of the fluorophores, to identify microscopic rate constants, and the conformational motions occurring within this enzyme. Significant changes in the fluorescence emission of the probes upon binding of IGP and substrate analog rCdRP were used to determine the binding parameters of the ligands. A mechanism was proposed for the pathway employed by SsIGPS, and was subsequently used to fit STO data for each labeled construct in a global fit using the DynaFit Program, to generate rate constants. Subsequently a mechanism for the conformational motion was proposed and the change in fluorescence intensity versus time data for the labeled constructs was fitted to this mechanism. Kinetic and conformational motion rate constants obtained from the fits were compared to fully map the entire catalytic pathway employed by SsIGPS and to determine the involvement of conformational motions in catalysis.

MONTCLAIR STATE UNIVERSITY

Conformational Motion Associated With Catalysis in Indole-3-glycerol phosphate synthase from *S. Solfataricus*

by

Tomasz Kurcon

A Master's Thesis Submitted to the Faculty of

Montclair State University

In Partial Fulfillment of the Requirements

For the Degree of

Master of Science, Concentration in Biochemistry

May 2010

College of Science and Mathematics

Department of Chemistry and Biochemistry

[redacted]

Robert Prezant, PhD.
Dean of College of Science and Mathematics

5/14/10
Date

Thesis Committee:

[redacted] 05/13/2010

Nina M. Goodey, PhD.
Thesis Sponsor

[redacted] 5/13/2010

Johannes P. Schelvis, PhD.
Committee Member

[redacted] 5/13/2010

John J. Siekierka, PhD.
Committee Member

[redacted] 5/13/10

Marc L. Kasner, PhD.
Department Chair

Conformational Motion Associated With Catalysis in Indole-3-glycerol Phosphate Synthase from *S. solfataricus*

A Thesis

Submitted in partial fulfillment of the requirements

For the degree of Master of Science

by

Tomasz Kurcon

Montclair State University

Department of Chemistry and Biochemistry

Montclair, NJ

2010

Acknowledgements

I would like to thank my parents Elzbieta and Tadeusz Kurcon whose hard work allowed me to pursue career in science and my brother Piotr Kurcon for continuous support throughout my years of study. I would like to thank Dr. Nina M. Goodey sponsor of this thesis, for reviewing my work, providing ribbon diagram of SsIGPS and exceptional guidance throughout the years of research summarized in this paper. I thank the committee Dr. Johannes Schelvis and Dr. John Siekierka for critical discussion. I thank Dr. Reinhard Sterner, Susanne Dietrich and Sandra Schlee for help with data analysis and for providing our lab with purified constructs as well as ligands. I would like to thank NSF funded GK-12 program for providing me with a stipend that allowed me to focus solely on research. Finally I thank Heba Obeidallah and Ruqaiya Naqvi for performing equilibrium titrations for ligand binding studies.

Contents:

	Abstract	I
	Thesis signature page	II
	Title page	III
	Acknowledgements	IV
	Contents	V
1.	**Introduction**	1
2.	**Abbreviations**	5
3.	**Materials and Methods**	6
	3a. Rates of reaction of cysteine residues with DTNB	6
	3b. Protein labeling and purification	6
	3c. Steady-state enzyme kinetics	7
	3d. Single turnover experiments	8
	3e. Multiple turnover experiments	9
	3f. Kinetics of ligand binding	9
	3g. Measurement of ligand binding equilibrium constants	10
4.	**Results**	11
	4a. Rates of reaction of cysteine residues with DTNB	11
	4b. Effect of labeling on enzymatic activity	12
	4c. Choice of fluorophore	13
	4d. Protein labeling and purification	14
	4e. Steady-state enzyme kinetics	16
	4f. Measurement of ligand binding equilibrium constants	18
	4g. Kinetics of ligand binding	19
	4h. Single turnover experiments	22
	4i. Multiple turnover experiments	35
5.	**Discussion**	37
6.	**References**	42
7.	**Appendix A**	44
8.	**Appendix B**	48
9.	**Appendix C**	52

1. Introduction

The $(\beta\alpha)_8$- barrel structure is a common motif in the broad family of TIM-barrel enzymes. Eight parallel β-strands, each connected to an α-helix by a βα loop, constitute eight βα units of a typical $(\beta\alpha)_8$- barrel structure. Despite chemically diverse reactions catalyzed by TIM-barrel enzymes, the active site residues of all known TIM-barrel enzymes are located on the C-termini of some of the parallel β-strands and some βα loops (*1*). Indole-3-glycerol phosphate synthase from *Sulfolobus solfataricus* (SsIGPS) is a TIM-barrel enzyme that catalyzes the fifth reaction in tryptophan biosynthesis, the conversion of 1-(o-carboxylphenylamino)-1-deoxyribulose-5-phosphate (CdRP) to indole-3-glycerol phosphate (IGP). Although, X-ray crystallography, thermostability and activity studies have been previously described for this enzyme, and general mechanism of action has been proposed (*1-4*), it is imperative to identify microscopic rate constants as well as conformational motions associated with catalysis to fully grasp the complex relationship between structure and catalytic capability of this $(\beta\alpha)_8$- barrel enzyme.

In addition to its remarkable stability, SsIGPS is a good model enzyme for studying the relationship between catalysis and dynamic motions. The active site of the enzyme is in part constructed by flexible loops and the motion of these loops, and perhaps the entire structure, are likely to be involved in catalysis. It is possible to detect conformational motion by monitoring changes in the emission intensity of environmentally sensitive fluorescent probes, such as the commercially available dyes PyMPO and Alexa Fluor 555. Upon conformational change, the probe might be buried or become exposed to solvent resulting in a decrease or an increase in the intensity of the fluorescence signal. A similar effect is observed upon change in polarity: the probe might be displaced into a more hydrophobic or hydrophilic environment (*5-6*). Attaching the probe to a flexible part of the protein, such as a βα loop, maximizes the chances to observe motion. Since it is experimentally easier to attach a probe to a position with high surface accessibility, Swiss PDB Viewer program was used by Dr. Nina M. Goodey to determine solvent accessibility of various residues. Asp61 on the β1α1 loop, Thr186 on the β6α6 loop and Arg18

k_{cat} of the enzyme by 20-fold and increases the Michaelis constant K_M^{CdRP} by 2000-fold, showing that this residue is essential for catalysis and that the β1α1 loop plays an important role in catalysis (*4*). Evidence of different conformational states and the importance of the β1α1 loop in catalysis render Asp61 a good choice for probe attachment for the purposes of this study.

Similarly, position 186 is expected to exhibit catalysis related conformational motion since Arg182 and Leu184 are involved in formation of the anthranilate-binding pocket and Leu184 is also involved in formation of the indole-binding pocket (*4*). It is reasonable to assume that motion in this loop would correlate to steps in catalysis since two of the amino acids in near proximity of Thr186 form the binding pocket. SsIGPS carries an N-terminal extension of about 40 residues that includes the α0 helix and α00 helix connected by the α0α00 loop. Studies of the truncated version of SsIGPS, SsIGPSΔ(1-26) where the entire α0 helix and first half of the α0α00 loop are removed, show that deletion of this motif has no effect on the core of the enzyme. The truncated version of the enzyme retained catalytic activity, but the K_M^{CdRP} value increased more than 3000-fold in comparison to the wild type SsIGPS (*1*). The radical increase in K_M^{CdRP} of the truncated version of the enzyme implies the role of the α0α00 loop in overall flexibility of the protein and suggests that its motions may play a role in catalysis.

In this thesis, it is shown how SsIGPS variants with single amino acid substitution were labeled with environmentally sensitive fluorophores, and their kinetic and conformational parameters were explored. Often an enzyme catalyzed reaction is composed of multiple steps that take place before the final product is formed. Each of the steps is essentially a sub-reaction with its own characteristic rate, leading closer to the formation of the product. Furthermore shape changes also known as conformational motions in the enzyme may proceed, accompany or follow each individual sub-reaction. Changes in 3D shape similarly to the sub- reactions have their own rates. This project attempts to identify a number of sub-reactions and shape changes during SsIGPS catalysis as well as their rates and determine whether there is a correlation between the sub-reactions and shape changes. Two distinct conformational motions correlating to steps in

catalysis were observed, and their rate constants were determined. The most probable mechanism employed by SsIGPS for catalysis of CdRP to IGP is proposed.

The goals of this study can be summarized as:

1. Successful labeling of constructs
2. Characterization of steady-state enzyme kinetics parameters
3. Determination of k_{on}, k_{off} and K_d for ligands (rCdRP and IGP)
4. Identification of microscopic rate constants for catalysis and conformational motion under single turnover (STO) experimental conditions
5. Identification of microscopic rate constants for catalysis and conformational motion under multiple turnover (MTO) experimental conditions
6. Proposition of catalytic mechanism employed by SsIGPS
7. Successful fitting of STO and MTO data to the proposed mechanism
8. Establish degree of involvement of conformational motion in catalysis
9. Generalization of SsIGPS results to other enzymes

2. Abbreviations

Alexa Fuor 555 – Alexa Fluor 555 Maleimide

PyMPO– 1-(2-maleimidylethyl)-4-(5-(4-methoxyphenyl)oxazol-2-yl)pyridiniummethanesulfonate (PyMPO) maleimide

R18C – single SsIGPS mutant; Arg18 was replaced by cysteine

D61C – single SsIGPS mutant; Asp61 was replaced by cysteine

T186C – single SsIGPS mutant; Thr186 was replaced by cysteine

R18C-T186C – double SsIGPS mutant; Arg18 and Thr186 were both replaced by cysteine

D61C-R18C – double SsIGPS mutant; Asp61 and Arg18 were both replaced by cysteine

T186C-D61C – double SsIGPS mutant; Thr186C and Asp61 were both replaced by cysteine

R18C^{PyMPO}– R18C labeled with PyMPO

R18C^{Alexa555}– R18C labeled with Alexa Fluor 555

D61C^{PyMPO} – D61C labeled with PyMPO

D61C^{Alexa555} – D61C labeled with Alexa Fluor 555

STO – single turnover conditions

MTO– multiple turnover condition

3. Materials and Methods

3a. Rates of reaction of cysteine residues with DTNB

Second order rate constants were determined for the reaction of cysteine variants with 5,5'-dithiobis-(2-nitrobenzoic acid(DTNB). The data was generated with SX20 Applied Photophysics stopped-flow instrument and fitted to single exponential equations to determine the second order rate constants with the program DynaFit. Reaction was initiated by mixing R18C (9.6 μM), D61C (8.1 μM) or T186C (7.74 μM) variant with DTNB (0.25 – 1.25 mM) in 1:1 volume:volume ratio, in 20 mM HEPES 5.0 mM EDTA, pH 7.2 and at room temperature. Progress curves were generated by measuring the increase in absorbance of the reaction product TNB^- at 412 nm (ε_{TNB^-} = 14.15 $mM^{-1}*cm^{-1}$) with time. Progress curves generated for different concentrations were fitted in a global fit using DynaFit Program to determine second order rate constants for the covalent bond formation between DTNB and a given cysteine.

3b. Protein labeling and purification

Protein constructs (R18C, D61C and T186C) were stored in a 100 mM potassium phosphate buffer pH 7.5 and 2 mM dithiothreitol (DTT). DTT was removed prior to labeling to prevent covalent attachment of DTT to the thiol-reactive probes Alexa Fluor 555 C_2 maleimide (Alexa Fluor 555 maleimide; Invitrogen, Cat. No. A-20346) and 1-(2-maleimidylethyl)-4-(5-(4-methoxyphenyl)oxazol-2-yl)pyridinium methanesulfonate (PyMPO maleimide; Invitrogen, Cat. No. M-6026). To remove DTT, the protein solution was diluted in the labeling buffer, 20 mM HEPES containing 5.0 mM EDTA pH 7.2, and concentrated using Amicon Ultra-15 micro concentrator (centrifugation: 5000 rpm at 4 °C) until the concentration of DTT was below 4 nM. Subsequently, 1.5 fold excess of the dye (Alexa Fluor 555 maleimide or PyMPO maleimide dissolved in DMSO) was added to the washed construct (protein concentration in the reaction: 50- 100 μM). The solution was allowed to react at room temperature for two hours and stored overnight at 4 °C. All steps involving the dye were performed in the dark to avoid

photobleaching; reaction vessel was protected from light by covering it in foil. Excess dye was removed by washing the reaction mixture three times with the reaction buffer and then with 100 mM HEPPS containing 10 % glycerol pH 7.5 (storage buffer) until the absorbance of free dye from the flowthrough measured at 556 nm (Alexa Fluor 555 maleimide) or 412 nm (PyMPO maleimide) was below the detection limit of Nanodrop 2000. Quantification of labeled constructs and the degree of labeling were determined using Nanodrop 2000. Extinction coefficient at 280 nm for each fluorophore was determined experimentally using the Nanodrop 2000 and pure dye dissolved in DMSO: $\varepsilon_{280\ nm} = 1414.7\ \mu M^{-1}*mm^{-1}$ (Alexa Fluor 555 maleimide) $\varepsilon_{280\ nm} = 1225.74\ \mu M^{-1}*mm^{-1}$ (PyMPO). Contribution to absorbance at 280 nm from each probe was calculated using Beer's law. Protein concentration was quantified using the corrected absorbance at 280 nm and previously determined extinction coefficient of the constructs (R18C, D61C and T186C) at 280 nm: $\varepsilon_{280\ nm} = 2040\ \mu M^{-1}*mm^{-1}$(*2*).

3c. Steady-state enzyme kinetics

Steady-State parameters were determined at 22 – 25 °C in 50 mM HEPPS buffer pH 7.5 containing 4.0 mM EDTA. FluoroMax-4 spectrophotometer (Horiba) was used to measure initial velocities at varying substrate concentrations. Progress curves were generated by measuring increase in emission intensity of product IGP at 340 nm (10 nm em. slit) after excitation at 280 nm (5 nm ex. slit). The reaction progress was measured for 30 seconds. Initial velocity data was plotted against CdRP concentration to derive saturation curves, which were subsequently fitted to the Michaelis-Menten equation in KaleidoGraph to generate K_M and V_{max} for SsIGPS and each labeled construct. The catalytic parameter k_{cat} was obtained by dividing V_{max} by total enzyme concentration. *Thermatoga maritime* IGPS (TmIGPS), which essentially bears no product inhibition, was used to find the relationship between fluorescence signal intensity and IGP concentration which in turn correlates directly to the concentration of the total CdRP which was converted to IGP by TmIGPS. Change in fluorescence signal was determined by mixing 50 nM

TmIGPS with varying concentrations of CdRP and allowing the reaction to go to completion. Linear analysis of the change in fluorescence vs. CdRP concentration generated a slope with units of CPS/μM, which was used as a conversion factor to convert a change in fluorescence emission intensity to IGP concentration. The stoichiometry for the reaction is 1:1; one CdRP molecule is converted to one IGP molecule. Initial velocities (μM IGP/sec produced or μM CdRP/sec consumed) were obtained by dividing the initial rates (CPS/sec) from the reaction catalyzed by SsIGPS and labeled SsIGPS constructs ($R18C^{Alexa555}$, $R18C^{PyMPO}$, $D61C^{Alexa555}$ and $D61C^{PyMPO}$) by the conversion factor (CPS/μM).

3d. Single turnover experiments

All experiments were performed at 25 °C in 50 mM HEPPS buffer pH 7.5 containing 4.0 mM EDTA. SX20 stopped-flow instrument (Applied Photophysics) was used to detect reaction progress after mixing $R18C^{Alexa555}$, $R18C^{PyMPO}$, $D61C^{Alexa555}$ or $D61C^{PyMPO}$ (12 – 16 μM) with CdRP (2.0 – 4.0 μM) in 1:1 volume:volume ratio. Increase in the emission intensity of the product IGP was collected with 320 nm cutoff filter after excitation of IGP at 280 nm. Subsequently, the reaction was repeated, this time monitoring the change in the emission intensity collected with 550 nm cutoff filter upon excitation of the probe at 514 nm (Alexa Fluor 555 maleimide) or 412 nm (PyMPO maleimide). A minimum of 4 traces was collected for each enzyme/substrate concentration. Signal from the buffer, ligands and the free protein was collected in the same manner. Signal of the buffer was subtracted from the signal of the ligands and the free protein. Next, the corrected signals for the CdRP and free protein were divided by their corresponding concentrations to obtain responses with the unit of (μM^{-1}) required for the fitting process. Data for each construct was fitted in a global fit using the DynaFit program. In the fitting script, experimentally determined responses were fixed while the responses for the complexes (ES and EP) were estimated based on the change in fluorescence signal observed during binding

studies. Throughout the fitting process the responses for the ES and EP as well as EI species were relaxed.

Table 1. Summary of concentrations used in single turnover experiments.

Construct	E/S (μM)	E/S (μM)	E/S (μM)	E/S (μM)	E/S (μM)
$R18C^{Alexa555}$	8/2	8/1	7/1	6/2	6/1
$R18C^{PyMPO}$	8/2	8/1	7/1	6/2	6/1
$D61C^{Alexa555}$	8/2	8/1	7/1	6/2	6/1
$D61C^{PyMPO}$	8/2	8/1	7/1	6/2	6/1

Summary of enzyme and substrate concentrations used for the single turnover experiments. E, corresponds to the final concentration of the labeled construct in the reaction cell, while S, corresponds to a final concentration of the substrate in the reaction cell. Protein and substrate were mixed in 1:1 volume:volume ratio at 25 °C in 50 mM HEPPS and 4.0 mM EDTA pH 7.5.

3e. Multiple turnover experiments

Pre-steady state kinetics of SsIGPS labeled constructs were explored under multiple turnover conditions. All experiments were performed at 25 °C in 50 mM HEPPS buffer pH 7.5 containing 4.0 mM EDTA. Mixing of $R18C^{Alexa555}$, $R18C^{PyMPO}$, $D61C^{Alexa555}$ or $D61C^{PyMPO}$ (1.0 μM) with CdRP (10 μM) in 1:1 ratio, initiated the reaction and the accumulation of the product IGP was monitored by exciting IGP at 280 nm and collecting the emission with 320 nm cutoff filter. Subsequently the experiment was performed again observing change in emission of the dye with 550 nm cutoff filter after excitation at 514 nm (Alexa Fluor 555 maleimide) or 412 nm (PyMPO maleimide).

3f. Kinetics of ligand binding

Stopped-flow studies were performed at 25 °C in 50 mM HEPPS buffer pH 7.5and 4.0 mM EDTA using the SX20 stopped-flow instrument (Applied Photophysics). Change in the emission intensity of the probe upon ligand binding was recorded over time after mixing $R18C^{Alexa555}$, $R18C^{PyMPO}$, $D61C^{Alexa555}$ or $D61C^{PyMPO}$ (0.2 μM) with IGP or CdRP (2-16 μM) in 1:1 ratio. Change in the emission intensity of each fluorophore was recorded with 550 nm cutoff filter after excitation at 295 nm (both probes), 412 nm (PyMPO maleimide) and 514 nm (Alexa Fluor

555 maleimide). For each ligand concentration, the average of at least four traces was fitted to a single exponential equation in ProData Viewer, to obtain k_{obs}. A plot of k_{obs} vs. ligand concentration was generated for each labeled construct and fitted to a linear equation in Excel, to generate binding parameters k_{on} (slope) and k_{off} (y-intercept). Free R18C^{PyMPO} was observed to have slight increase in the emission intensity upon mixing with the buffer. To account for this increase, during binding studies with R18C^{PyMPO}, an average of a minimum of 4 traces generated in the absence of the ligand was subtracted from progress curves prior to fitting with ProData Viewer.

3g. Measurement of ligand binding equilibrium constants

Fluorescence titrations were performed at 25 °C in 50 mM HEPPS buffer pH 7.5 and 4.0 mM EDTA using the FluoroMax-4 instrument (Horiba). Small aliquots of IGP or rCdRP were added to a cuvette containing 1.1 μM labeled construct and mixed. The complex was equilibrated for 40 seconds before signal was collected. For R18C^{Alexa555} and D61C^{Alexa555} signal was collected at 564 nm (10 nm em. slit.) after excitation at 295 nm (1 nm ex. Slit) and at 564 nm (4 nm em. slit) after excitation at 514 nm (1 nm ex. Slit). For R18C^{PyMPO} and D61C^{PyMPO} the signal was collected at 561 nm (10 nm em. slit) after excitation at 295 nm (3 nm ex. slit). Minimum of three titrations were performed. Each of the titrations was corrected by subtracting the average of at least three titrations of protein with buffer (collected under identical conditions as corresponding titration with the ligands) and fitted to Equation 1 in KaleidoGraph.

$$\frac{[RL]}{[R]} = \delta = \frac{([R] + [L] + \mathrm{K_d}) - \sqrt{([R] + [L] + K_d)^2 - 4[R][L]} * (\delta_{\mathrm{bound}} - \delta_{\mathrm{free}})}{2[R]} + \delta_{\mathrm{free}}$$

Equation 1. Equation used to fit corrected fluorometric titrations of labeled constructs with IGP or rCdRP.

4. Results

4a. Rates of reaction of cysteine residues with DTNB

To determine the optimum labeling conditions for the SsIGPS single mutants (R18C, D61C and T186C), second order rate constants for the reaction of cysteine with DTNB were determined for each mutant using the SX20 stopped-flow instrument, and modified published protocol (*8*). Global analysis of absorbance versus time data under varying concentration of DTNB in DynaFit program (*9*) (Figure 2) indicated that R18C SsIGPS, the most slowly reacting variant, reacts at a rate that is one order of magnitude slower than that for D61C SsIGPS and T186C SsIGPS Table 2. Time constants of the reaction spanned a range from 150 ms (T186C SsIGPS) to 28 000 ms (R18C SsIGPS) indicating high reactivity for both variants. This is concordant with the design of the variants, where each cysteine was introduced in one of the three loops near the active site, each easily accessible to the solvent. Fast reactivity of each cysteine handle enables quick and efficient labeling of the constructs.

Originally, the intention was to generate SsIGPS construct with a covalently attached FRET pair. Therefore, to ascertain that the rates are unaffected by the presence of another cysteine in near proximity, rates of reaction with DTNB were also determined for the double mutants (D61C-T186C, R18C-D61C and T186C-R18C). Global analysis of absorbance versus time data under varying concentration of DTNB in DynaFit program indicated that the rates were not affected by the presence of another nearby cysteine in the three double mutants (data not shown). The observed ten-fold difference in reactivity of cysteine handles at position 18 and the two cysteines at positions 61 and 186 would allow for highly selective labeling reaction. Conversely small difference between reactivity of cysteine handles at position 61 and 186 would require a highly sensitive separation method to ensure selective labeling.

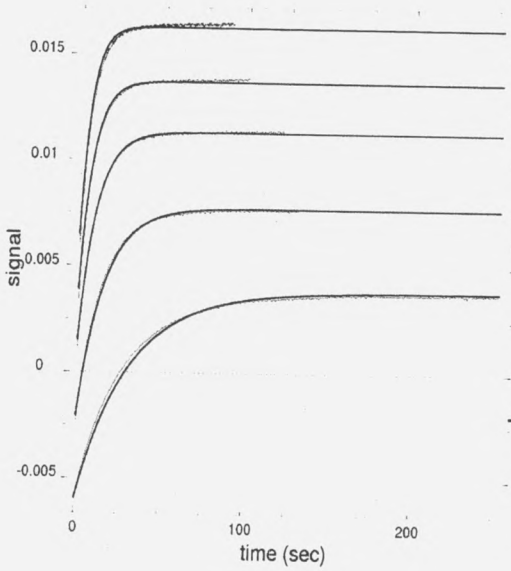

Table 2. Thiol reactivity of cysteine handles

construct	cysteine position	k ($mM^{-1}*s^{-1}$)
R18C	18	0.261
D61C	61	2.65
T186C	186	3.48

Thiol reactivity constants were determined by measuring k_{obs} under varying DTNB concentrations followed by global fit of the data in DynaFit program. Detailed conditions are specified in Materials and Methods section.

Figure 2. Representative global fit generated in DynaFit Program for the reaction of 4.1 μM R18C and 0.25-1.25mM DTNB (final) at room temperature in 20 mM HEPES buffer, 5.0 mM EDTA, pH 7.2.

4b. Effect of labeling on enzymatic activity

The three single mutants were labeled with Alexa Fluor 555 maleimide to generate the controls ($R18C^{Alexa555}$, $D61C^{Alexa555}$ and $T186C^{Alexa555}$) and were subsequently assayed for activity using fluorescence spectrophotometer and SX20 stopped flow instrument (Figure 3). Activity of $R18C^{Alexa555}$ and $D61C^{Alexa555}$ were not affected by the probe as they were found to have a very similar activity to the wild type enzyme. $T186C^{Alexa555}$ shows more than a ten-fold decrease in activity when compared to the wild type SsIGPS (Figure 3). Due to radical decrease in activity of T186C after labeling, use of this construct as a model for wild type SsIGPS is very limited. As a result of observing this drop in activity, constructs containing the T186C mutation were eliminated from the study because, upon labeling, they would not have activity resembling that of the native protein. The results may suggest that labeling SsIGPS at position 186, located closer to the active site than position 18 or position 61, could partially block the access of the substrate CdRP or hinder the release of the product IGP.

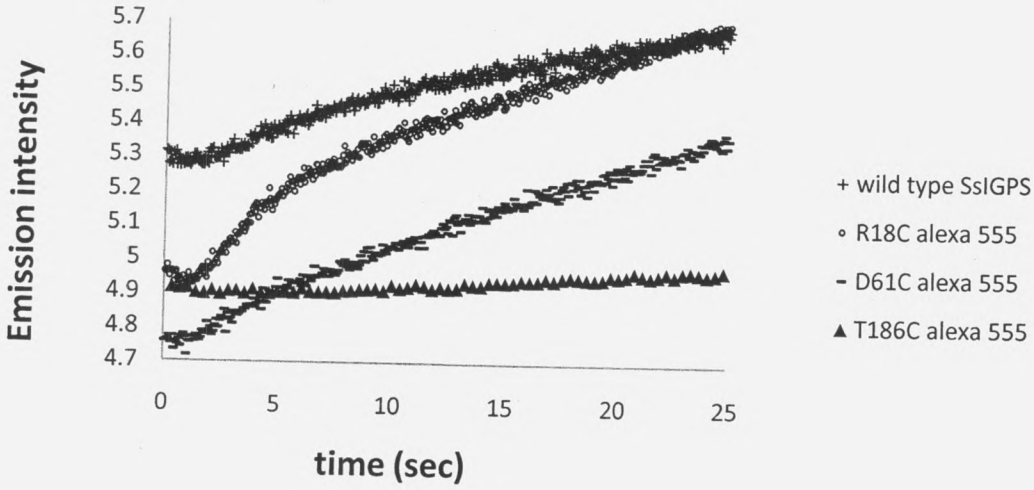

Figure 3. Stopped-flow generated traces reflecting activity of the wild type SsIGPS and labeled constructs. Progress curves were generated by mixing 23 nM enzyme with 2.3 μM CdRP in 1:1 ratio at 19.7 °C in 50 mM HEPPS buffer pH 7.0 containing 4.0 mM EDTA and 1.0 mM DTT. Increase in the formation of IGP was observed with 320 nm cutoff filter upon excitation at 280 nm.

4c. Choice of fluorophore

Originally Alexa Fluor 555 maleimide was chosen as a part of a FRET pair and single SsIGPS constructs: R18C, D61C and T186C were designed to be controls for the experiment. D61C was labeled with Alexa Fluor 555 maleimide and was used to characterize fluorescent properties of the dye in that region, by mixing 23 nM $D61C^{Alexa555}$ with 2.3 μM CdRP and collecting emission intensity with 550 nm cutoff filter upon excitation at 514 nm. Significant change in fluorescence of Alexa Fluor 555 maleimide upon catalysis (Figure 4A), indicates that the environmental sensitivity of the dye is sufficient to study conformational motion without the need of generating a FRET pair. In order to increase the validity of the study, PyMPO maleimide, another environmentally sensitive probe was selected in an attempt to duplicate the study using another probe. D61C was labeled with PyMPO maleimide and fluorescent properties of the probe were characterized by mixing 23 nM $D61C^{PyMPO}$ with 2.3 μM CdRP and exciting the dye at 412 nm while collecting emission with 550 nm cutoff filter. As expected, a significant change in fluorescence of PyMPO maleimide was observed upon catalysis as shown in Figure 4B.

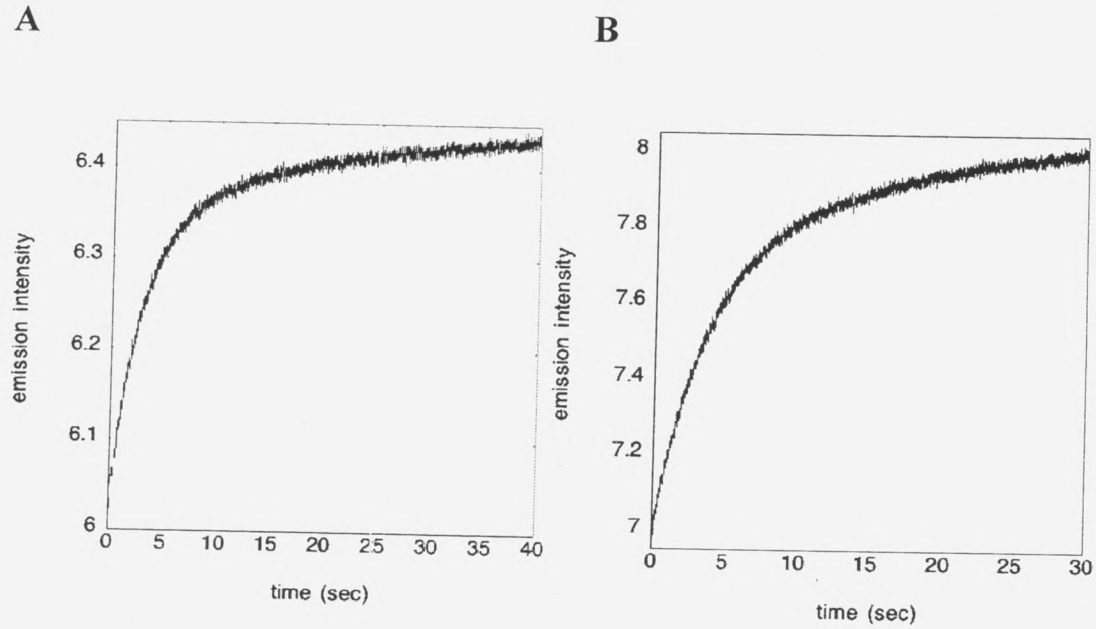

Figure 4. Fluorescence emission intensity vs. time data for D61C labeled with (A) Alexa Fluor 555 and (B) PyMPO observed after mixing of 23 nM D61C$^{Alexa555/PyMPO}$ and 2.3 μM CdRP in 1:1 ratio at 20 °C in 50 mM HEPPS buffer pH 7.0 containing 4.0 mM EDTA and 1.0 mM DTT.

4d. Protein labeling and purification

All labeled single amino acid replacement constructs were created by incubating the enzyme and Alexa Fluor 555 dye with 3 fold molar excess of the dye to protein at room temperature in 20 mM HEPES buffer pH 7.2 and 5.0 mM EDTA for two hours. The excess dye was diluted out using an Amicon Ultra 15 concentrator and the protein was analyzed for elution pattern with FPLC using a SOURCE Q15 anion exchange resin. Negatively charged Alexa Fluor 555 increases the affinity of labeled protein for the resin, enabling good separation (Figure 5). Labeled constructs were equilibrated in the column with 50 mM Tris-HCl buffer pH 8.5 and eluted with a 0.0-0.5 M NaCl gradient over 100 mL (in the same buffer). Positively charged arginine replaced by cysteine in the R18C SsIGPS construct slightly increased affinity of this mutant for the resin compared to wild type SsIGPS. On the contrary, the D61C SsIGPS construct, where negatively charged aspartic acid was replaced by a cysteine, was found to have slightly lower affinity for the SOURCE Q15 resin. However, unlabeled R18C and D61C both elute at

approximately 0.09 M NaCl. Negatively charged Alexa Fluor 555 increases affinity of both constructs for the positively charged resin and therefore D61C^{Alexa555} SsIGPS elutes at 0.12 M NaCl and R18C^{Alexa555} SsIGPS elutes at 0.16 M NaCl. Subsequent analysis, employing the same resin, of labeling reactions performed at varying protein to dye ratios and equilibration time revealed optimum labeling conditions. All subsequent labeling reactions were performed with these optimal conditions: 1.5 fold molar excess of the dye in 20 mM HEPES buffer pH 7.2. The reaction was equilibrated at room temperature for two hours and placed at 4 ˚C overnight. The following day, excess dye was diluted out using an Amicon Ultra 15 concentrator. Successive FPLC chromatograms did not show peaks corresponding to unlabeled protein indicating levels well under the detection limit of the instrument (data not shown).

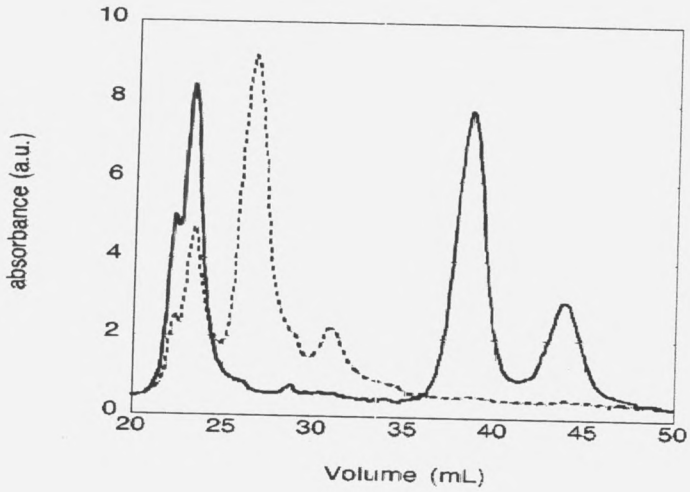

Figure 5. Elution pattern of D61C (dotted line) and R18C (solid line) labeled with Alexa Fluor 555. First peak, overlap of R18C and D61C corresponds to unlabeled constructs which have lower affinity for the column and elute at 0.09 M NaCl, followed by two doublets correlating to D61C^{Alexa555} (eluted at 0.12 M NaCl) and R18C^{Alexa555} (eluted at 0.16 M NaCl) respectively. Data for T186C^{Alexa555} not shown.

Concentration of labeled protein was determined using the Nanodrop 2000 spectrophotometer; the absorbance was measured both at 280 nm (maximum absorbance for protein) and 556 nm (maximum absorbance for Alexa Fluor 555). Molar extinction coefficient $\varepsilon_{280\ nm}$ of Alexa Fluor 555 was determined experimentally in the following manner: absorbance of 30X dilution in distilled water of 1 mg/mL Alexa Fluor 555 in DMSO was measured at 280 nm

and 556 nm using Nanodrop 2000. The molar extinction coefficient of Alexa Fluor 555 at 280 nm was calculated using Equation 2.

$$\varepsilon_{280\text{ nm Alexa Fluor 555}} = \frac{A_{280}}{A_{556}} * \varepsilon_{556\text{ nm Alexa Fluor 555}} \qquad \text{Equation 2}$$

The molar extinction coefficient of Alexa Fluor 555 at 280 nm ($\varepsilon_{280\text{ Alexa Fluor 555}}$ = 1414.7 $M^{-1}mm^{-1}$) was used to determine contribution of absorbance of the dye at 280 nm to the absorbance of the labeled protein construct. Molar extinction coefficient of PyMPO at 280 nm was calculated in the same way ($\varepsilon_{280\text{ PyMPO}}$ = 1225.74 $M^{-1}mm^{-1}$) and used to account for the contribution of absorbance at 280 from the dye to the labeled construct. Contribution to absorbance at 280 nm from protein was determined using Beer's law and Equation 3.

$$A_{280\text{ protein}} = A_{280\text{ total}} - A_{280\text{ dye}} \qquad \text{Equation 3}$$

Following the correction of absorbance at 280 nm, Beer's law was used to determine the total protein concentration with previously determined extinction coefficient for wild type SsIGPS $\varepsilon_{280\text{ protein}}$ = 2040 $M^{-1}mm^{-1}$(*2*). The degree of labeling was calculated by dividing the total concentration of the dye by the total concentration of the protein. Labeled construct was deemed acceptable for use in subsequent experiments if the degree of labeling was above 90 % or if the dye was in less than 5 % excess. Following absorbance measurements, labeled protein was aliquoted and stored in 100 mM HEPPS buffer pH 7.5 with10 % glycerol.

4e. Steady-state enzyme kinetics

Steady-state enzyme kinetic studies were undertaken to compare the wild type enzyme with the labeled constructs $R18C^{Alexa555}$, $R18C^{PyMPO}$, $D61C^{Alexa555}$and $D61C^{PyMPO}$ SsIGPS. The turnover numbers (k_{cat}), Michaelis constants (K_M^{CdRP}) as well as the catalytic efficiency parameters, summarized in Table 3, were derived from fitting substrate saturation curves (Figure

6) to the Michaelis-Menten Equation (Equation 4). Steady-state parameters k_{cat} as well as the K_M^{CdRP} of the wild type SsIGPS were found to be concordant with values reported in literature validating the experimental protocol (*1,2*). Presence of a probe in the $R18C^{PyMPO}$, $R18C^{Alexa555}$ and $D61C^{Alexa555}$ SsIGPS constructs resulted in a 40 % decrease in the k_{cat} and K_M^{CdRP} values. Slightly smaller k_{cat} (slower enzyme) and smaller K_M (improved binding to CdRP) of the three labeled mutants resulted in similar overall catalytic efficiency (k_{cat}/K_M^{CdRP}) to the wild type SsIGPS enzyme. Slight increase in the value of K_M for the $D61C^{PyMPO}$ indicated looser binding to CdRP.

$$V = V_{max}[S]/(K_M + [S])$$ Equation 4

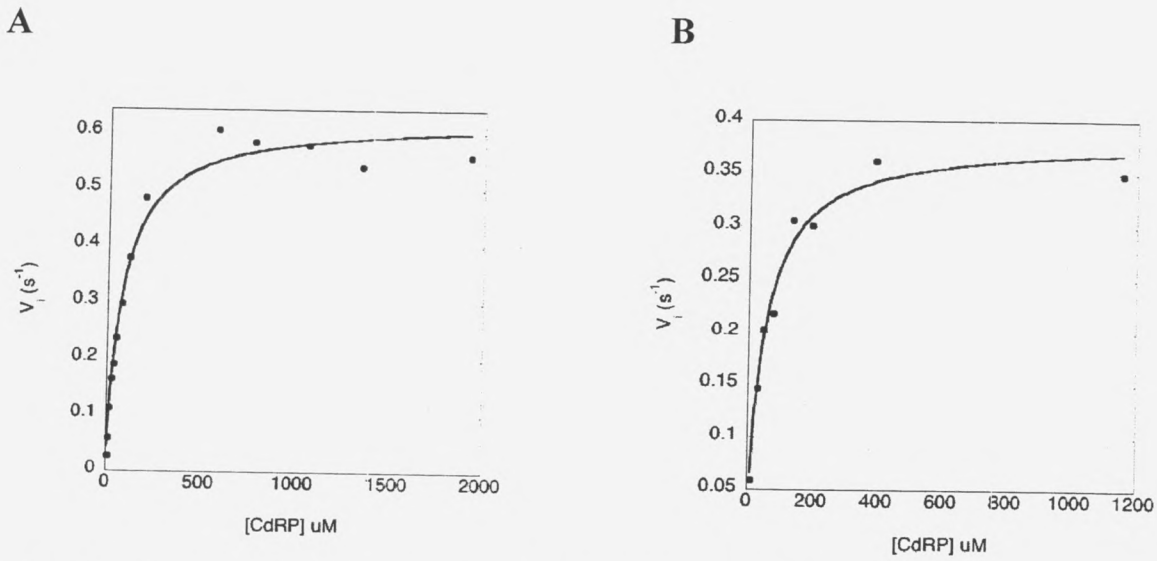

Figure 6. Steady-state kinetic parameters of the wild type SsIGPS and labeled constructs were determined using FluoroMax-4 fluorescence spectrophotometer. Enzyme (10 nM) was mixed with 50 – 10,000 nM CdRP at 22-25 °C in 50 mM HEPPS buffer pH 7.5 containing 4.0 mM EDTA and 1.0 mM DTT. Increase in fluorescence emission at 340 nm (10 nm em. slit) upon excitation of the product IGP at 280 nm (5 nm ex. slit) was measured for 30 seconds. Initial velocities were converted to $nM*s^{-1}$ by dividing slopes by experimentally determined conversion factor, 8506 $CPS*nM^{-1}$. The conversion factor was obtained as specified in the Materials and Methods section: steady-state enzyme kinetics. Representative fits: (A) wild type SsIGPS was fitted to Michaelis-Menten equation (Equation 4) to generate $k_{cat} = 0.062\ s^{-1}$ and $K_M = 80$ nM, (B) $D61C^{Alexa555}$ was fitted to Michaelis-Menten equation to generate $k_{cat} = 0.038\ s^{-1}$ and $K_M = 46$ nM. Similar velocity versus [CdRP] plots were obtained for the other constructs; the results are shown below in Table 3.

Table 3. Summary of steady-state kinetic parameters K_M and k_{cat} generated for wild type SsIGPS and labeled constructs after fitting data to Equation 4 using the KaleidoGraph program.

Enzyme	k_{cat} (s^{-1})	error (k_{cat})[a]	K_M (nM)	error (K_M)	k_{cat}/K_M ($\mu M^{-1}s^{-1}$)
wild type SsIGPS	0.062	± 0.002	80	± 9	0.78
$D61C^{Alexa555}$	0.038	± 0.001	46	± 7	0.83
$D61C^{PyMPO}$	0.065	± 0.002	109	± 11	0.60
$R18C^{Alexa555}$	0.042	± 0.001	50	± 8	0.84
$R18C^{PyMPO}$ *	0.040	± 0.001	45	± 5	0.89

Initial rates were determined by fitting progress curves to a linear equation. Progress curves were generated after mixing of 10 nM enzyme with 50 – 10,000 nM CdRP at 22-25 °C in 50 mM HEPPS buffer pH 7.5 containing 4.0 mM EDTA and 1.0 mM DTT, and observing increase in fluorescence emission for 30 seconds at 340 nm (10 nm em. slit) upon excitation of the product IGP at 280 nm (5 nm ex. slit). * no DTT in the reaction buffer. [a]Error in regression.

4f. Measurement of ligand binding equilibrium constants

Equilibrium dissociation constants K_d were determined by equilibrium binding studies using fluorescence measurements. Increasing concentration of the ligand was added to a fixed concentration of $R18C^{PyMPO}$, $D61C^{PyMPO}$ or $D61C^{Alexa555}$ SsIGPS. Experiments with $R18C^{Alexa555}$ were not yet performed. The fluorescence of the solution containing the ligand and labeled protein (excitation 295 nm, emission 550 nm) exceeded that of separately measured protein (true for construct labeled with PyMPO and Alexa Fluor 555) indicating that the quantum yield of the fluorophore is higher in the protein-ligand complex than in the absence of bound ligand. Significant quenching in the intrinsic fluorescence of the probes was observed over the duration of the titration experiment. The binding curve in Figure 7 was obtained by subtracting the signal of the titration performed in absence of the ligand from the signal of a titration performed in presence of the ligand. This correction was done for all the titration experiments. Values of K_d obtained by fitting corrected saturation curves to Equation 1 are summarized in Table 4.

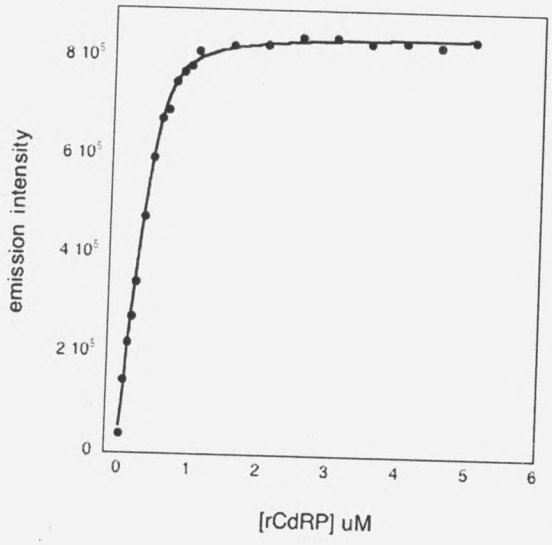

Figure 7. Representative emission intensity versus ligand concentration data from fluorometric titration of D61C^{PyMPO} SsIGPS with rCdRP at 25 °C in 50 mM HEPPS, 4.0 mM EDTA, pH 7.5. Fluorescence (ex. 295 nm, slit 3 nm / em. 561 nm, slit 10 nm) was used to detect increase in the formation of the enzyme-rCdRP complex upon increasing concentrations of rCdRP. To correct the signal for quenching, the average of three titration curves of protein with buffer (no rCdRP) was subtracted from each of the three protein-rCdRP titration curves. The three individual corrected titration curves were fitted to Equation 1, and the three resulting equilibrium dissociation constants were averaged to give K_d= 0.032 μM ± 0.0098. K_d values are summarized in Table 4.

Table 4. Equilibrium and rate constants for binding of IGP and rCdRP to labeled D61C and R18C

		Equilibrium[a]		Rate[b]	
Construct	**Ligand**	**K_d (μM)**	**Standard Deviation (K_d)**	**k_{on} ($\mu M^{-1}S^{-1}$)**	**k_{off} (s^{-1})**
D61C^{Alexa555}	IGP	0.029	± 0.022	3.47	0.101
D61C^{Alexa555}	rCdRP	0.126	± 0.023	1.97	0.236
D61C^{PyMPO}	IGP	0.028	± 0.0026	1.36	0.034
D61C^{PyMPO}	rCdRP	0.032	± 0.0098	0.596	0.018
R18C^{PyMPO}	IGP			5.49	
R18C^{PyMPO}	rCdRP	0.092		3.72	0.32

Equilibrium and rate constants for binding of IGP and rCdRP to D61C^{Alexa555} and D61C^{PyMPO}. Values of k_{off} were calculated from the relationship $k_{off} = K_d * k_{on}$. All experiments were run at 25 °C in 50 mM HEPPS, 4.0 mM EDTA pH 7.5. [a] conditions as specified in the legend of Figure 7. [b] conditions as specified in the legend of Figure 8. [c]

4g. Kinetics of ligand binding

The bimolecular association of the substrate analog rCdRP (Figure 15) and the product IGP can be observed by measuring the time dependent change in fluorescence intensity of the probes Alexa Fluor 555 and PyMPO. The binding was examined by observing change in emission intensity of the probes (550 nm cutoff filter) upon excitation at 295 nm (both probes),

514 nm (Alexa Fluor 555) or 412 nm (PyMPO) using SX20 stopped flow instrument. To ensure saturation of protein, ligand concentrations several orders of magnitude greater than the equilibrium dissociation constant were used. Moreover, pseudo first order conditions under which concentration of one of the reactants during the course of reaction does not change with respect to the other reactant, were achieved by varying ligand concentration between 10-80 fold higher than protein concentration. The time course of binding of rCdRP and IGP to labeled construct is characterized by a single exponential phase that requires 2-10 s for completion at the lowest ligand concentration. A representative fluorescence trace of measurement of ligand association with $D61C^{Alexa555}$ is shown in Figure 8.

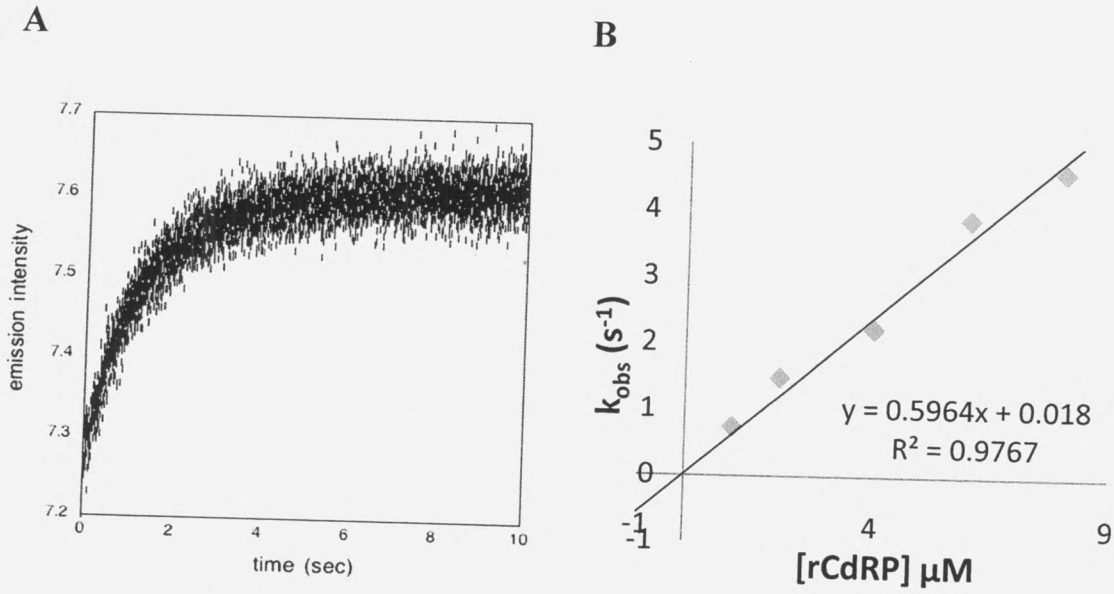

Figure 8. Kinetics of rCdRP binding to $D61C^{PyMPO}$. Experiments were performed in 50 mM HEPPS buffer, 4.0 mM EDTA, pH 7.5 at 25 °C. $D61C^{PyMPO}$ SsIGPS was mixed in an Applied Photophysics SX20 stopped flow instrument with IGP or rCdRP in 1:1 ratio to give final concentrations of 0.1 μM of protein and 1 – 8 μM of ligand (IGP or rCdRP). (A) Typical single exponential fluorescence increase observed upon binding of 1 μM rCdRP (final) to 0.1 μM $D61C^{PyMPO}$ (final concentrations). Progress curve was fitted to a single exponential equation to obtain k_{obs} = 0.74 s^{-1}. (B) Plot of k_{obs} versus total concentration of rCdRP in the cell in μM. The data was fitted to Equation 6 to obtain a preliminary k_{on} value (0.559 $\mu M^{-1}s^{-1}$). The k_{off} value was calculated using the preliminary k_{on} value and the K_d value obtained from ligand binding titrations described above. The k_{obs} versus rCdRP concentration data was then fitted to a Equation 6, fixing the y-intercept to the calculated k_{off} value (0.018 s^{-1}). The value for k_{on} (0.596 $\mu M^{-1}s^{-1}$) was obtained from the slope of this fit. Fixing the y-intercept to the calculated k_{off} value did not significantly change the R^2 or k_{on} values compared to those obtained from the original linear fit to the data. The values of rate constants are provided in Table 4.

Experiments were run in duplicate, using excitation wavelength of 295 nm (both probes) and two different emission wavelengths: 514 nm (Alexa Fluor 555) and 412 nm (PyMPO). For each experiment in a set a minimum of 3 to 4 traces were averaged to generate a single progress curve. Values of observed rates (k_{obs}) were determined by fitting progress curves to Equation 5

$$\delta = Ae^{(-kt)} + c$$

Equation 5

where δ is the change in fluorescence, A corresponds to the amplitude of the signal and c is corresponds to the signal maximum. Subsequently data for k_{obs} versus ligand concentration was fitted to the linear equation (Equation 6) to obtain preliminary k_{on} from the slope (Figure 7B). Because small value of k_{off} cannot be determined from the ordinate line intercept as accurately as the k_{on} from the slope of the line, k_{off} was calculated using Equation 7where K_d is the equilibrium dissociation constant (Table 4).

$$K_{obs} = k_{off} + k_{on}[\text{Ligand}]$$

Equation 6

$$k_{off} = k_{on} * K_d$$

Equation 7

The k_{obs} versus ligand concentration data was fitted again to Equation 5, constraining the y-intercept to calculated k_{off}, to obtain final value of k_{on} that was within 10 % difference in comparison to k_{on} determined without restraining the k_{off}. The k_{on} values were reproducible between different excitation wavelengths, however significant variation in values of k_{off} was observed when comparing data obtained from signal excited at 295 nm and that obtained by exciting fluorescence at 514 nm or 412 nm. Moreover, increase in fluorescence emission of the free $R18C^{PyMPO}$ upon mixing with buffer was observed when exciting PyMPO at 412 nm. To account for this increase in emission intensity, the binding traces were corrected by subtracting

signal of the free protein. Furthermore, progress curves generated by exciting the probes at 514 nm (Alexa Fluor 555) and 412 nm (PyMPO) were observed to have double exponential character for lower concentrations of the ligands, but were single exponentials for higher concentrations of the ligands. This discrepancy was not observed when exciting at 295 nm.

Careful examination of emission and excitation spectra of the ligands and the probes (data not shown) revealed spectral overlap between the emission of the ligands and the excitation of the probes (at higher wavelengths). Thus when exciting at 295 nm we are exciting not only PyMPO and Alexa Fluor 555 but rCdRP and IGP as well. Excitation of rCdRP and IGP leads to fluorescence energy transfer from the ligands to the probes significantly contributing to the emission of each fluorophore. It appears that measuring binding using 295 nm excitation wavelength allows for more sensitive and accurate measurements.

4h. Single turnover experiments

The next step in the kinetic analysis of the wild type SsIGPS and labeled SsIGPS constructs ($R18C^{Alexa555}$, $R18C^{PyMPO}$, $D61C^{Alexa555}$ and $D61C^{PyMPO}$ SsIGPS) was to determine microscopic rate constants (a rate constant for each step in a single reaction) for individual reaction rates catalyzed. SX20 stopped-flow instrument was used to measure time dependent change in fluorescence emission intensity upon mixing of substrate with an excess of labeled enzyme construct; detailed conditions are described in Table1 of the Materials and Methods section. In order to map the entire catalytic pathway employed by SsIGPS, catalysis of CdRP to IGP was observed by monitoring time dependent change in the emission intensity of CdRP and IGP with 320 nm cutoff filter upon excitation at 280 nm, while conformational motion was studied by monitoring time dependent change in emission intensity of the fluorophores with 550 nm cutoff filter upon excitation at 514 nm (Alexa Fluor 555) or 412 nm (PyMPO). When protein undergoes conformational motion the fluorophore might be displaced in a different environment

resulting in change of the signal, thus change in emission intensity of the probe is directly related to the conformational motion.

All experiments were run in duplicate, first by observing formation of IGP followed by observing conformational motion associated with catalysis. For each experiment set a minimum of 4 traces was averaged to generate one progress curve. Progress curves reflecting formations of IGP were found to be biphasic for all labeled constructs ($D61C^{Alexa555}$, $D61C^{PyMPO}$, $R18C^{Alexa555}$ and $R18C^{PyMPO}$ SsIGPS) (Figure 9A), and characterized by an initial shallow decrease followed by a more profound increase. Traces reflecting conformational motion (probe emission) in $D61C^{Alexa555}$ SsIGPS and $R18C^{PyMPO}$ SsIGPS were also characterized by initial decrease, followed by a much stronger increase (Figures 13A and 10A respectively). On the other hand, fluorescence emission of $D61C^{PyMPO}$ SsIGPS showed a biphasic increase (Figure 12A), while fluorescence emission of $R18C^{Alexa555}$ SsIGPS was characterized by a double exponential decrease when observing probe emission (Figure 11A).

Control experiments were conducted to rule out contribution of CdRP binding in the kinetic traces. STO experiments were replicated using unreactive substrate analog rCdRP instead of substrate CdRP and the progress curves generated by observing time dependent change in fluorescence were compared in order to rule out correlation of the signals. The rCdRP binding curves observed with 320 nm cutoff filter upon excitation at 280 nm were characterized by single exponential increase for all labeled constructs ($R18C^{Alexa555}$, $R18C^{PyMPO}$, $D61C^{Alexa555}$ and $D61C^{PyMPO}$ SsIGPS) (Figure 9B).

Since the first phase of the progress curves reflecting formation of the product IGP are characterized by initial decrease, it is safe to conclude that binding of CdRP is not observed during catalysis under STO conditions described in this paper. This makes sense because opposite signals are observed for the binding event and the first step following formation of the enzyme-CdRP complex.

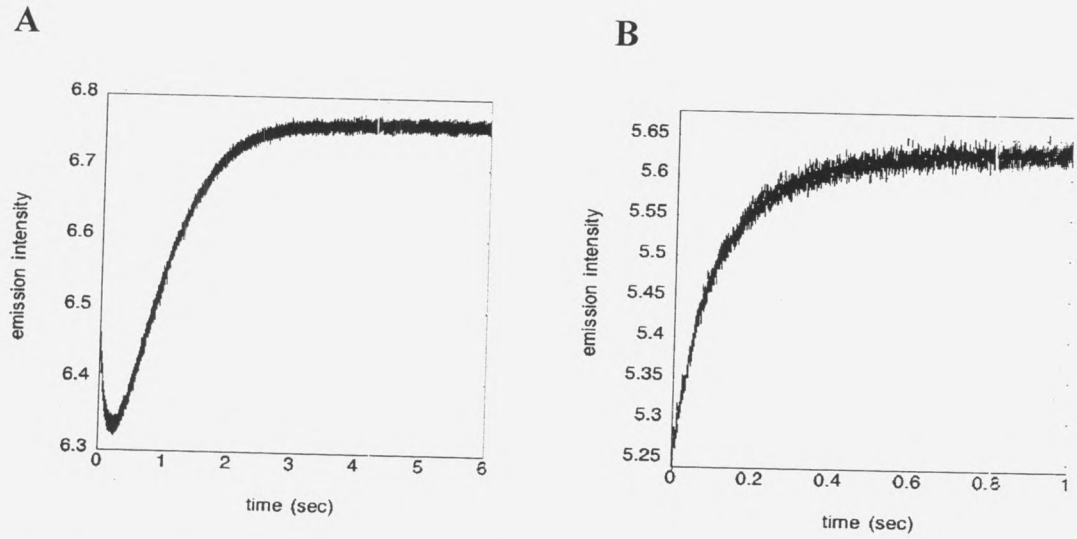

Figure 9. Progress curves generated under single turnover conditions after mixing R18C^{PyMPO} SsIGPS and CdRP or rCdRP in 1:1 ratio to give final concentrations of 6 μM R18C^{PyMPO} SsIGPS and 1 μM CdRP or 1 μM rCdRP. Experiments were performed at 25 °C in 50 mm HEPPS pH 7.5 and 4.0 mM EDTA. Emission intensity was collected with 320 nm cutoff filter upon excitation at 280 nm; the same PM voltage was used when observing catalysis of CdRP and binding of rCdRP. (A) Typical progress curve generated for catalysis of CdRP to product IGP by R18C^{PyMPO} SsIGPS. This type of biphasic curve was observed for all labeled constructs (R18C^{Alexa555}, R18C^{PyMPO}, D61C^{Alexa555} and D16C^{PyMPO} SsIGPS) at conditions specified above, where initial shallow fluorescence emission decrease was followed by more distinct fluorescence emission increase. (B) Conformational motion associated with binding of rCdRP to R18C^{PyMPO} SsIGPS under STO conditions. Parallel STO experiments were run using rCdRP instead of CdRP to determine whether it is possible to observe binding under STO conditions described in the materials and methods section. Similar type of increase in fluorescence emission was observed upon rCdRP binding for all the constructs. Since opposite fluorescence signals during binding and catalysis were observed, it is safe to conclude that the initial signal decrease observed for the CdRP catalysis under STO conditions is not binding.

Subsequently conformational motion associated with rCdRP binding was measured under STO conditions and was compared with conformational motion detected during catalysis of CdRP. Increase in the emission intensity of PyMPO was observed upon binding of rCdRP to R18C^{PyMPO} SsIGPS (Figure 9B). Since conformational motion observed in R18C^{PyMPO} SsIGPS during catalysis of CdRP is characterized by an initial decrease in fluorescence of PyMPO, ligand binding cannot be solely responsible for the trace in Figure 9A.

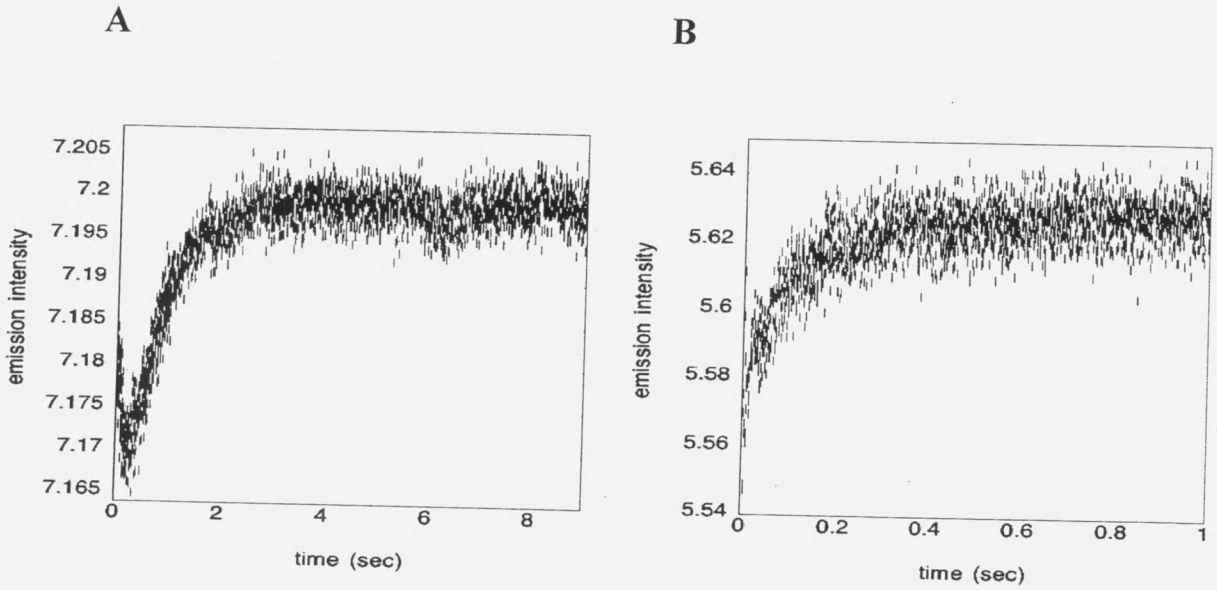

Figure 10. Progress curves generated under single turnover conditions after mixing R18C^{PyMPO} SsIGPS and CdRP or rCdRP in 1:1 ratio to give final concentrations of 6 μM R18C^{PyMPO} SsIGPS and 1 μM CdRP or 1 μM rCdRP. Experiments were performed at 25 °C in 50 mm HEPPS pH 7.5 and 4.0 mM EDTA. Emission intensity was collected with 550 nm cutoff filter upon excitation at 412 nm; the same PM voltage was used when observing conformational motion associated with catalysis of CdRP and binding of rCdRP (notice different x-axis (time) scales for the two plots). (A) Time dependent change in fluorescence emission of PyMPO maleimide observed upon catalysis of CdRP to product IGP by R18C^{PyMPO} SsIGPS. Similar conformational motion characterized by biphasic change in emission intensity of the probe was also observed for D61C^{Alexa555} SsIGPS at conditions specified above, where initial emission decrease was followed by more distinct fluorescence emission increase. (B) Conformational motion associated with binding of rCdRP was used as control to determine whether binding of CdRP is detected in conformational motion curves determined under STO conditions (A).Since opposite fluorescence signals during binding and catalysis were observed, it is safe to conclude that the initial signal decrease observed for the CdRP catalysis under STO conditions is not binding.

On the other hand, for R18C^{Alexa555} SsIGPS, a similar decrease in emission intensity of Alexa Fluor 555 was observed for rCdRP binding to R18C^{Alexa555} SsIGPS and conformational motion during catalysis of CdRP, indicating that similar motions are being detected by the probe in this construct during ligand binding and catalysis (Figure 11). Since similar rate constants and signal amplitudes were observed for rCdRP binding (double exponential fit provided $k_1 = 1.8\ s^{-1}$, $k_2 = 8.6\ s^{-1}$) and CdRP catalysis ($k_1 = 1.1\ s^{-1}$, $k_2 = 8.6\ s^{-1}$), it is safe to conclude that the only conformational motion observed in R18C^{Alexa555} SsIGPS during catalysis (under STO conditions) is CdRP binding.

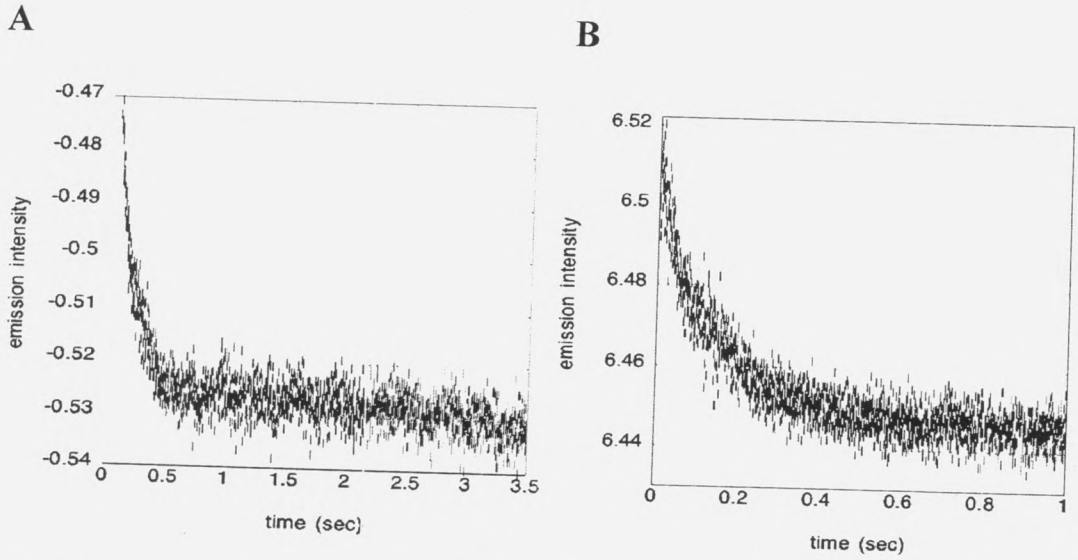

Figure 11. Progress curves generated under single turnover conditions after mixing R18C^{Alexa555} SsIGPS and CdRP or rCdRP in 1:1 ratio to give final concentrations of 6 μM R18C^{Alexa555} SsIGPS and 1 μM CdRP or 1 μM rCdRP. Experiments were performed at 25 °C in 50 mm HEPPS pH 7.5 and 4.0 mM EDTA. Emission intensity was collected with 550 nm cutoff filter upon excitation at 514 nm; the same PM voltage was used when observing conformational motion associated with catalysis of CdRP and binding of rCdRP. (A) Time dependent change in fluorescence emission of Alexa Fluor 555 maleimide observed upon catalysis of CdRP to product IGP by R18C^{Alexa555} SsIGPS (signal was corrected by subtracting signal from free protein). (B) Conformational motion associated with binding of rCdRP was used as control to determine whether binding of CdRP is detected in conformational motion curves generated under STO conditions (A). Progress curve reflecting conformational motion associated with catalysis (A) and that associated with rCdRP binding (B) were fitted to a two step mechanism. The resulting rates are very similar (conformational motion k_1 = 1.8 s^{-1}, k_2 = 8.6 s^{-1}; rCdRP binding, k_1 = 1.1 s^{-1}, k_2 =8.6 s^{-1}) indicating that during CdRP catalysis the only conformational motion observed is the conformational motion associated with substrate binding.

Contribution of binding to traces reflecting conformational motion in D61C^{PyMPO} SsIGPS was eliminated based on differences in signal and rates (Figure 12). A decrease in the emission intensity of Alexa Fluor 555 was observed for the conformational motion observed upon binding of rCdRP to D61C^{Alexa555} SsIGPS and the conformational motion during catalysis of CdRP by D61C^{Alexa555} SsIGPS. Fitting of the emission intensity versus time data generated rate constants different enough to rule out CdRP binding as the sole contributor to conformational motion trace in Figure 13.

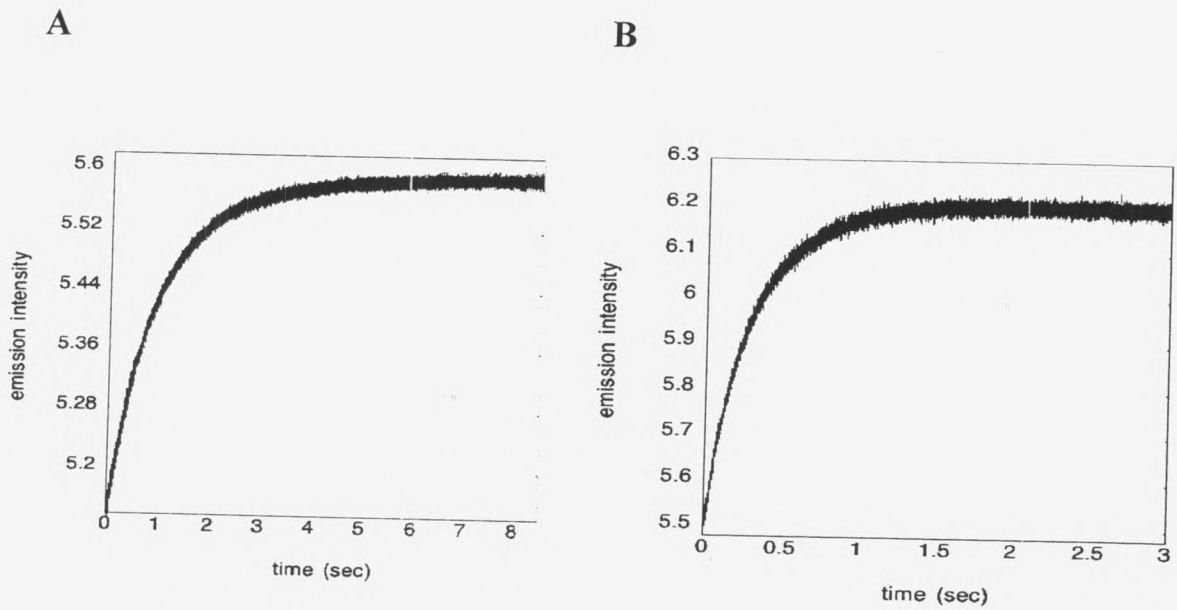

Figure 12. Progress curves generated under single turnover conditions after mixing D61C^{PyMPO} SsIGPS and CdRP or rCdRP in 1:1 ratio to give final concentrations of 6 μM D61C^{PyMPO} SsIGPS and 1 μM CdRP or 1 μM rCdRP. Experiments were performed at 25 °C in 50 mm HEPPS pH 7.5 and 4.0 mM EDTA. Emission intensity was collected with 550 nm cutoff filter upon excitation at 412 nm; the same PM voltage was used when observing conformational motion associated with catalysis of CdRP and binding of rCdRP. (A) Time dependent change in fluorescence emission of PyMPO maleimide observed upon catalysis of CdRP to product IGP by D61C^{PyMPO} SsIGPS. (B) Conformational motion associated with binding of rCdRP was used as control to determine whether binding of CdRP is detected in conformational motion curves determined under STO conditions. Exploring conformational motion associated with CdRP catalysis by D61C^{PyMPO} SsIGPS on a millisecond timescale shows a shallow decrease in the beginning of the progress curve. Since such decrease was not observed in the binding of rCdRP binding to D61C^{PyMPO} under STO conditions, contribution of binding of CdRP to D61C^{PyMPO} SsIGPS in traces reflecting conformational motion under STO conditions can be temporally eliminated. Furthermore the resulting rates are different (conformational motion associated with catalysis of CdRP $k_1 = 0.7\ s^{-1}$, $k_2 = 2\ s^{-1}$; rCdRP binding, $k_1 = 1.2\ s^{-1}$, $k_2 = 4.3\ s^{-1}$) indicating that different conformational motions are observed during catalysis of CdRP and rCdRP binding.

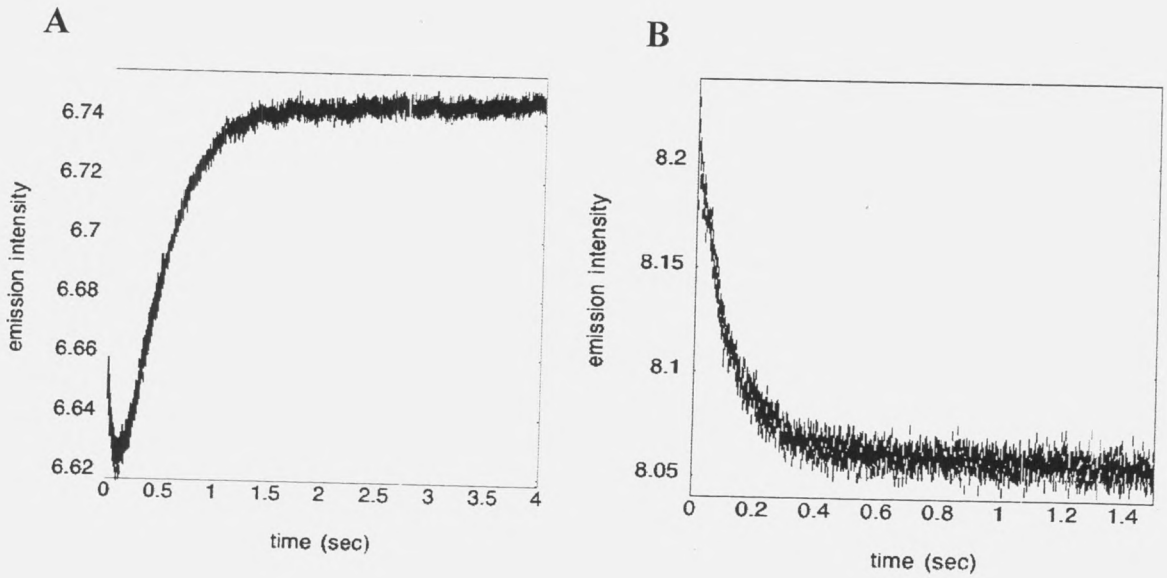

Figure 13. Progress curves generated under single turnover conditions after mixing D61C^{Alexa555} SsIGPS and CdRP or rCdRP in 1:1 ratio to give final concentrations of 6 μM D61C^{Alexa555} SsIGPS and 1 μM CdRP or 1 μM rCdRP. Experiments were performed at 25 °C in 50 mm HEPPS pH 7.5 and 4.0 mM EDTA. Emission intensity was collected with 550 nm cutoff filter upon excitation at 514 nm; the same PM voltage was used when observing conformational motion associated with catalysis of CdRP and binding of rCdRP. (A) Time dependent change in fluorescence emission of Alexa Fluor 555 maleimide observed upon catalysis of CdRP to product IGP by D61C^{Alexa555} SsIGPS. (B) Conformational motion associated with binding of rCdRP was used as control to determine whether binding of CdRP is detected in conformational motion curves determined under STO conditions. Progress curves were fitted to determine whether the signal decrease observed upon rCdRP binding is the same as the initial signal decrease observed for conformational motion associated with catalysis. The resulting rates are different (catalysis of CdRP $k = 2.9\ s^{-1}$; rCdRP binding, $k = 7.3\ s^{-1}$) indicating that different conformational motions are observed during catalysis of CdRP and rCdRP binding.

Data generated under STO conditions was fitted in DynaFit program. While it is possible to fit progress curves observed under STO condition to multiple mechanisms, most of the mechanisms fail when fitting data obtained under varying conditions in a global fit. Thus, data measured under varying substrate and enzyme concentrations (Table 1) was fitted globally (all data obtained under different conditions must fit to a single mechanisms with a single set of rate constants). Prior to fitting, fluorescence responses (fluorescence/μM) for the species present in the solution (labeled protein, IGP, CdRP and the buffer) during catalysis were determined experimentally by collecting fluorescence emission intensity of each component in a buffer and

dividing the signal of the component alone (buffer signal was subtracted) by corresponding concentration to calculate the response with a unit of (μM^{-1}). Due to significant variation, experimentally determined responses could not always be constrained to a fixed number, but were used as guesses in the fitting process. The output responses would be considered acceptable if they were within 10% of the input responses (Table 5). Furthermore, it was possible to anticipate the output responses for the enzyme-substrate complex (ES) based on the signals observed in the binding study. Bimolecular association of rCdRP observed with 320 nm cutoff filter upon excitation at 280 nm is characterized by an increase in fluorescence (Figure 9B) and therefore the quantum yield of the complex E-rCdRP must be larger than that of the free enzyme and free ligand, indicating that the response for ES should be greater than the response for free S and free E. It was previously reported (*2*) that binding of IGP to wild type SsIGPS is also characterized by an increase in fluorescence emission (ex. 295 nm, em. 320 nm cutoff filter), however it was difficult to reproduce this increase upon excitation at 280 nm with the labeled constructs due to small signal amplitude, therefore responses for the E-IGP complex could not be anticipated the same way the responses for E-rCdRP complex were and were not restrained in the fitting process.

Table 5. Responses used in the fitting script for $D61C^{Alexa555}$ SsIGPS

Solution Component	**Input Response (μM^{-1})**	**Output Response (μM^{-1})**
Enzyme	0.730	0.728
Substrate	0.210	0.227
ES-complex	0.850	0.854
EI-complex	0.700	0.705
EP-complex	1.26	1.28
Product	1.55	1.53

This is summary of responses used in the fitting of $D61C^{Alexa555}$ SsIGPS data generated under STO conditions by following formation of IGP with 320 nm cutoff filter after exciting at 280 nm. Input responses were determined experimentally under the same conditions as STO experiments and were used as guesses in the fitting process. The output responses were provided as optimum responses by the program after fitting.

Previously determined kinetic parameters k_{on} and k_{off}, for IGP and rCdRP (Table 4) were constrained in the fitting scripts. In the fitting process of data for R18C^{PyMPO} SsIGPS, the catalytic turnover number k_{cat} was used as a guess for k_{off}, since the actual value had not yet been determined, and the catalytic turnover of the wild type SsIGPS was reported to be limited by the product release (*2*). Similarly, the k_{on} and k_{off} rates for binding of IGP and rCdRP to R18C^{Alexa555} SsIGPS had not yet been determined and therefore the same values that were used for R18C^{PyMPO} SsIGPS were also used to fit STO data for R18C^{Alexa555} SsIGPS. Due to the biphasic nature of IGP accumulation curves observed with 320 nm cutoff filter upon excitation at 280 nm, initially a mechanism with one intermediate was proposed (Scheme 1). Data for catalysis of CdRP to product IGP by labeled SsIGPS constructs was successfully fitted to this mechanism yielding three distinct microscopic rate constants. The best fits were obtained if the first step following binding was reversible (k_2, k_{-2}) and the consecutive step was irreversible (k_3). This mechanism makes sense since one of the steps in the reaction involves a decarboxylation, an irreversible step.

```
E + S <=====> ES      : k1   k-1
ES    <=====> EI      : k2   k-2
EI    ------> EI2     : k3
EP    <=====> E + P   : k4   k-4
```

Scheme 1. Mechanism used to fit IGP accumulation data determined under STO conditions in a global fit. In the mechanism k_1, k_{-4} and k_{-1}, k_4 correspond to k_{on} and k_{off}, respectively. The on and off rates were constrained to fixed, experimentally determined values summarized in Table 4. In the mechanism EI corresponds to enzyme intermediate (I) complex.

Subsequently, data for the conformational motion associated with catalysis of CdRP, observed by monitoring change in the emission intensity of the probes, was fitted to a two step mechanism, a mechanism with two forward rates leading to the formation of the product from the reactant via single intermediate, shown in Scheme 2. Similarly, the responses for the species present in the solution during catalysis under STO conditions were determined experimentally to

allow for fewer degrees of freedom during the fitting process, by measuring the emission intensity with 550 nm cutoff filter upon excitation at 514 nm (Alexa Fluor 555) or 412 nm (PyMPO). As expected, no signal was observed for the ligands IGP or rCdRP at these wavelengths. The response with the unit of (μM^{-1}) for the protein was obtained by dividing emission intensity signal by the total protein concentration; subtracting buffer signal before division was not necessary since there was no signal associated with the buffer at those wavelengths.

```
E  -----> E'    : k2'
E' -----> E''   : k4'
```

Scheme 2. Mechanism used to fit data for the conformational motion associated with catalysis, where E corresponds to E-CdRP complex conformer, while E' and E'' correspond to subsequent conformational states. Since ligands are not detected at the wavelengths used to observe motion, and binding was ruled out previously (Figures 9-12), binding and release steps were not included in the mechanism. For simplicity data was fitted to two irreversible steps since at STO conditions equilibrium significantly favors the forward reaction. The rate constants are summarized in Table 6. All scripts and their corresponding graphs are summarized in Appendix B. Representative graph for data generated for global fitting of data for $D61C^{Alexa555}$ is shown in Figure 14B.

Fitting conformational motion data (Figure 14B) for three labeled constructs ($R18C^{PyMPO}$, $D61C^{Alexa555}$ and $D61C^{PyMPO}$ SsIGPS) to the mechanism in Scheme 2 generated two microscopic rate constants for each construct (denoted with prime subscript), one of which ($k_{2'}$) correlated to k_2 (ES to EI) obtained from fits of IGP accumulation data. This indicates presence of a conformational motion that coincides with catalysis at the same rate as conversion of substrate to the first intermediate. The other rate constant for the second conformational motion $k_{4'}$ did not correlate to any of the rate constants generated for the IGP accumulation data. This was true for all labeled mutants except $R18C^{Alexa555}$ SsIGPS where no conformational motion associated with catalysis was detected other that conformational motion associated with binding of the ligands (Figure 11). Altogether there are three distinct microscopic rate constants measured in the

forward direction k_2 (same as $k_{2'}$ for the conformational motion), k_3 (IGP accumulation) and $k_{4'}$ (conformational motion). This indicates presence of two intermediates in the reaction mechanism as suggested by previously proposed mechanism (*3*) (Figure 15). Therefore, IGP accumulation data (ex. 280 nm, em. 320 nm cutoff filter) was fitted to a mechanism in Scheme 3 to see if the data could be fitted to a mechanism with two intermediates, and another rate constant $k_{4'}$ correlating to the second conformational motion, without changing rate constants obtained by fitting with simpler mechanism in Scheme 1. It is likely that $k_{4'}$ indicates presence of another intermediate since x-ray crystallography data of ligand-enzyme complexes (ES and EP) and computational modeling data for EI and EI2 suggest change in orientation of chemically important residues to accommodate second intermediate (*4*).

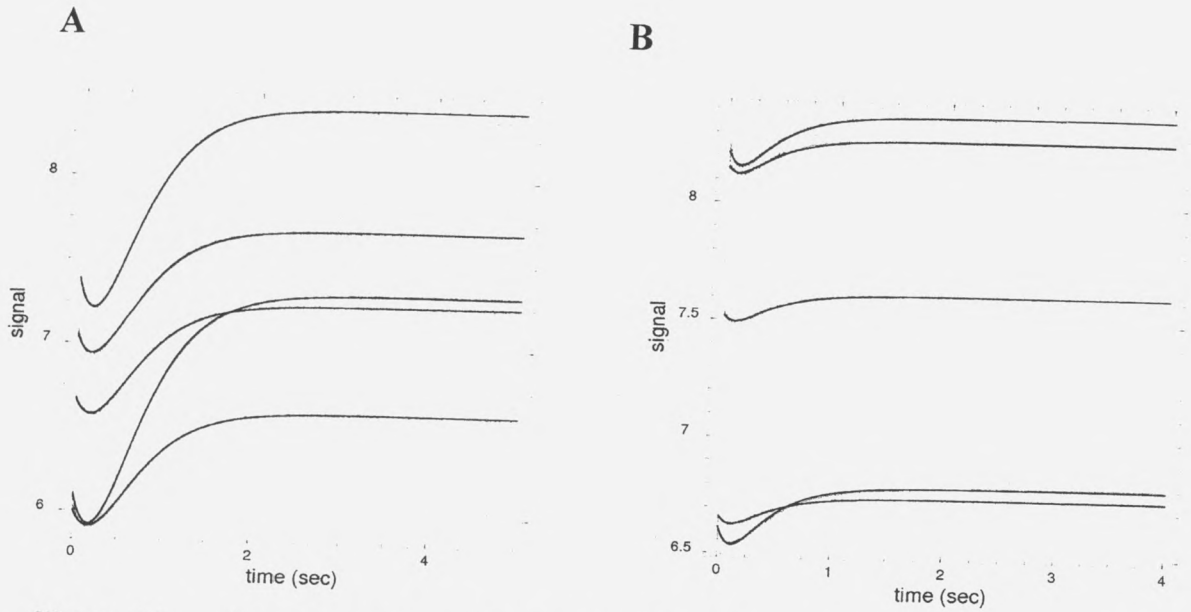

Figure 14. Progress curves generated with SX20 stopped-flow instrument after mixing D61C^{Alexa555} SsIGPS with CdRP in 1:1 ratio at 25 °C in 50 mM HEPPS, 4.0 mM EDTA pH 7.5 to give final concentration of 6-8 μM D61C^{Alexa555} SsIGPS and 1-2 μM CdRP. (A) Catalysis of CdRP by D61C^{Alexa555} was observed by monitoring increase in formation of IGP with 320 nm cutoff filter upon excitation of IGP at 280 nm. Fluorescence signal vs. time data was fitted in a global fit to the mechanism in Scheme 3A. Responses in the fitting script were determined experimentally as described in the Materials and Methods section. (B) Conformational motion associated with catalysis of CdRP to IGP by D61C^{Alexa555} SsIGPS observed by monitoring change in emission of Alexa Fluor 555 with 550 nm cutoff filter upon excitation at 514 nm. Fluorescence signal vs. time data was fitted to the mechanism in Scheme 2. All fitting scripts and corresponding graphs are summarized in Appendix A and B.

Since the rate constant for the first conformational motion ($k_{2'}$) correlates with the first rate constant measured for IGP accumulation (k_2), and binding of the substrate as well as the release of the product were not observed in the progress curves, there are only two possible mechanisms that can accommodate an extra step with a second intermediate (I2). In the first mechanism, the formation of complex with the second intermediate (EI2) is irreversible, and it is followed by reversible formation of the enzyme-product complex (EP) (Scheme 3A). In the second mechanism the formation of EI2 is reversible and it is followed by irreversible formation of the EP complex (Scheme 3B).

A

```
E + S <=====> ES      : k1   k-1
ES    <=====> EI      : k2   k-2
EI    ------> EI2     : k3
EI2   <=====> EP      : k4   k-4
EP    <=====> E + P   : k5   k-5
```

B

```
E + S <=====> ES      : k1   k-1
ES    <=====> EI      : k2   k-2
EI    <=====> EI2     : k4   k-4
EI2   ------> EP      : k3
EP    <=====> E + P   : k5   k-5
```

Scheme 3. Mechanism used to fit IGP accumulation data determined under STO conditions in a global fit. In the mechanism k_1, k_{-5} and k_{-1}, $k_5$correspond to k_{on} and k_{off} rates respectively. The on and off rates were constrained to a fixed experimentally determined values summarized in Table 4. (A) First possible mechanism including step with second intermediate complex EI2 (mechanism of choice). Microscopic rate constants k_2 - k_{-4} generated for each mutant are summarized in Table 6. Fitting scripts for each labeled construct and their corresponding graphs can be found in Appendix A. EI2 in the mechanism corresponds to the enzyme complex with the second intermediate I2. (B) Second possible mechanism including step with second intermediate EI2. Although it was possible to fit the data for three labeled constructs well to this mechanism, fitting of D61C^{PyMPO} data to this mechanism was unsuccessful.

IGP accumulation data for all labeled constructs could be fitted to the mechanism in Scheme 3A (Figure 14A), retaining rate constants obtained when fitting with mechanism in Scheme 1. Furthermore, the responses generated with this fit correlated well with experimentally determined responses. Although it was possible to fit STO data for R18C^{Alexa555}, R18C^{PyMPO} and D61C^{Alexa555} SsIGPS with mechanism in Scheme 3B, and retain previous rates and obtain reasonable responses, this mechanism failed to fit D61C^{PyMPO} SsIGPS data. Moreover, mechanism in Scheme 3A is concordant with mechanism previously proposed by Parry (*3*) for enzyme-catalyzed synthesis of indole ring (Figure 15).

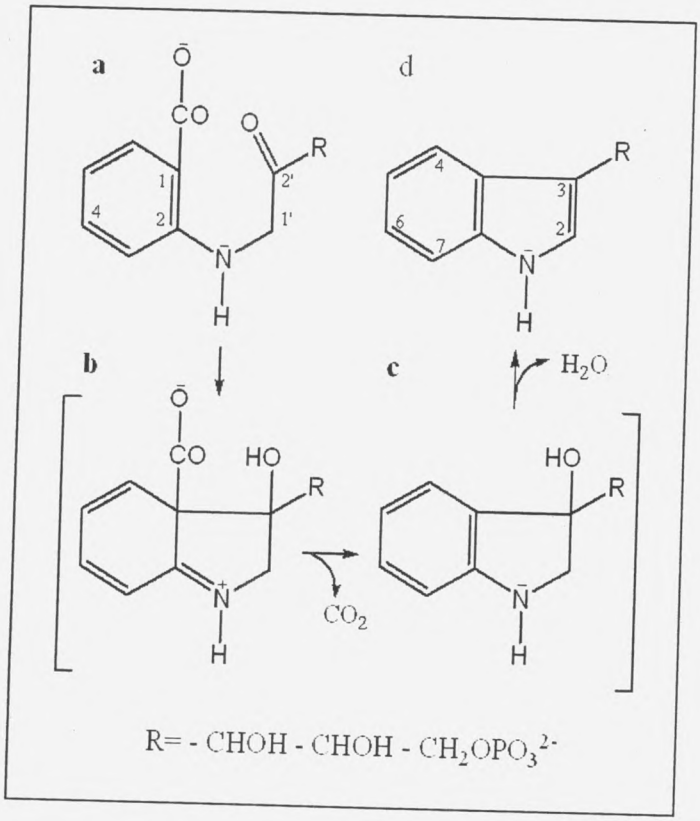

Figure 15. Enzyme-catalyzed synthesis of IGP proposed by Parry (*3*). (a) is the substrate CdRP. Substrate analog rCdRP carries OH-group at the 2' carbon of the CdRP. (b) First intermediate (I). (c) Second intermediate (I2). (d) Product IGP.

Mechanism in Scheme 3A is most likely the mechanism employed by SsIGPS. According to this mechanism after ES complex forms, the substrate is converted to the first intermediate, as the ES complex undergoes a conformational motion to form EI complex. No conformational motion was observed for the subsequent decarboxylation of the first intermediate to form the second intermediate, as the EI complex is converted to the EI2 complex. During the following dehydration step, EI2 complex undergoes conformational motion to form EP complex as the second intermediate is converted to the product. Thus k_2 is concordant with $k_{2'}$ and k_4 is concordant with $k_{4'}$. Rate constants obtained for conformational motion and product accumulation, are concordant with this mechanism and are summarized in Table 6.

Table 6. Summary of microscopic rate constants determined under single turnover conditions

	Product Accumulation					**Conformational Motion**	
Construct	k_2 (s^{-1})	k_{-2} (s^{-1})	k_3 (s^{-1})	k_4 (s^{-1})	k_{-4} (s^{-1})	$k_{2'}$ (s^{-1})	$k_{4'}$ (s^{-1})
$D61C^{Alexa555}$	2.7	0.002	3.2	7.9	0.46	2.9	9.2
$D61C^{PyMPO}$	1.7	0.02	12.2	0.52	0.04	2	0.67
$R18C^{Alexa555}$	1.9	4.0E-04	3.7	4.0	0.09	not obs	not obs
$R18C^{PyMPO}$	2	2.3E-03	3.1	4.1	0.08	1.6	5.8

All experiments were run at 25 °C in 50 mM HEPPS, 4.0 mM EDTA pH 7.5. For each construct a minimum of four traces (under each condition) was averaged and fitted in a global fit in DynaFit program to generate microscopic rate constants. The rate of the first conformational motion $k_{2'}$ corresponds to k_2, and the second conformational motion $k_{4'}$ corresponds to k_4. Scripts used in fitting and corresponding graphs can be found in the appendix section.

4i. Multiple turnover experiments

Pre-steady state multiple turnover kinetics under varying CdRP concentrations were explored for $D61C^{Alexa555}$ mutant. In the MTO experiments the substrate is in excess, allowing each enzyme to perform multiple conversions (turnovers) of substrate to product. The first turnover was observed by monitoring change in fluorescence emission on a millisecond timescale followed by consecutive turnovers. Both IGP accumulation and conformational motion associated

with catalysis were explored. Conformational motion data for the MTO experiments was analyzed in a global fit by fitting data to the mechanism in Scheme 2 in DynaFit program to determine whether varying CdRP concentration or consecutive turnovers affect the rate constants determined for the conformational motion studied under STO conditions above. The results of the fit are summarized in Table 7.

Table 7. Rate constants for the conformational motion determined under MTO conditions in D61C^{Alexa555}.

Conditions	$k_{2'}$ (s^{-1})	Error ($k_{2'}$)	$k_{4'}$ (s^{-1})	Error ($k_{4'}$)
MTO	3.1	0.001	13	0.01
STO	2.9	0.01	9.2	0.02

All experiments were run at 25 ^{0}C in 50 mM HEPPS buffer pH 7.5 and 4.0 mM EDTA. For each construct a minimum of four traces (under each condition) was averaged and fitted in a global fit in DynaFit program to generate microscopic rate constants. Scripts used in fitting and corresponding graphs can be found in Appendix C. Fitted traces were corrected for the signal from free protein.

The MTO experiments show that the motions observed in D61C^{Alexa555} during catalysis are CdRP concentration independent, suggesting that CdRP binding is not contributing to the conformational motion traces under the experimental conditions chosen for the study. Furthermore, it appears that the same rate constants are obtained during consecutive turnovers and during single turn over conditions when observing conformational motion. The same type of analysis must be performed for the IGP accumulation data under MTO conditions before the mechanism employed by this enzyme can be finalized. It is unlikely but possible that when observing IGP accumulation consecutive turnovers result in altered pre-steady state rate constants summarized in Table 6. If such discrepancy is observed, an alternative mechanism, fitting both STO and MTO data to the same rate constants must be proposed.

5. Discussion

It is essential to fully understand the role of conformational motion in enzyme catalysis not only to better understand remarkable catalytic capabilities of proteins but also to contribute indispensable information to the field of protein engineering and drug development. Understanding the role of conformational motion is crucial to the field of protein engineering because proteins are flexible structures and their structural changes may define their function (*15*). Moreover understanding conformational motion will enhance drug screening since structural changes may determine which compound is going to be compatible with the active site (*16*). Studying of the relationship between conformational motion and catalysis in SsIGPS will not only reveal full catalytic mechanism employed by this enzyme but may potentially allow for generalizations for other enzymes.

In order to fully understand catalysis it is important to know rates for each of the reaction steps such as conversion of substrate to the first intermediate. The rates for each individual step are called microscopic rates. In addition each of the steps may be proceeded, accompanied or followed by conformational motion therefore understanding these events is important to fully understand enzyme catalysis. Although it is possible to identify some microscopic rate constants by monitoring consumption of the substrate or formation of the product under STO conditions, some of the steps may not provide a signal in these experiments due to lack of distinct signal corresponding to the intermediates formed during a particular step in catalysis. In this study, environmentally sensitive probes Alexa Fluor 555 and PyMPO revealed the presence of another intermediate in the reaction catalyzed by SsIGPS that was not observed when following IGP accumulation alone. The substrate CdRP (Figure 15) is a weak fluorescent compound with an absorption maximum located in the UV range (*13*). It is possible to excite CdRP at 280 nm and follow its weak emission with a 320 nm cutoff filter. SsIGPS catalyzed conversion of CdRP to the first intermediate results in a loss of aromaticity, leading to a decrease in fluorescence emission intensity (Figure 9A). Subsequently, formation of the second intermediate restores

aromaticity leading to more fluorescent compound (*14*). Finally the highly fluorescent product IGP is formed by dehydration of the second intermediate. Increase in the fluorescence signal associated with the product may overpower emission of the second intermediate leading to a biphasic curve even when the reaction has two intermediates and three steps associated with chemical transformations (ES to EI, EI to EI2, and EI2 to EP) (Figure 9A).

Conformational motion studies under STO conditions using SsIGPS constructs labeled with environmentally sensitive probes revealed presence of two distinct conformational motions. One of the rates ($k_{2'}$) correlated with one of the steps in catalysis, but the other ($k_{4'}$) did not, indicating the presence of another rate in the apparently biphasic IGP accumulation curves. Rate constant $k_{4'}$ for the second conformational motion was successfully incorporated into the mechanism used to fit IGP accumulation data (Scheme 3A) without changing any of the rates, thus confirming the presence of another intermediate not observed when monitoring conversion of CdRP to product IGP using 320 nm cutoff filter (ex. at 280 nm). Although complete set of experiments under MTO conditions must be analyzed before final mechanism of action can be proposed for this enzyme, analysis of STO experiments strongly supports the following mechanism:

$$E + S \underset{k_{-1}}{\overset{k_1}{\rightleftharpoons}} ES \underset{k_{-2}}{\overset{k_2}{\rightleftharpoons}} EI \xrightarrow{k_3} EI_2 \underset{k_{-4}}{\overset{k_4}{\rightleftharpoons}} EP \underset{k_{-5}}{\overset{k_5}{\rightleftharpoons}} E + P$$

Table 8. Summary of microscopic rate constants determined under single turnover conditions for the SsIGPS catalyzed reaction using the mechanism above.

	Product Accumulation					**Conformational Motion**	
Construct	k_2 (s^{-1})	k_{-2} (s^{-1})	k_3 (s^{-1})	k_4 (s^{-1})	k_{-4} (s^{-1})	$k_{2'}$ (s^{-1})	$k_{4'}$ (s^{-1})
D61C^{Alexa555}	2.7	0.002	3.2	7.9	0.46	2.9	9.2
D61C^{PyMPO}	1.7	0.02	12.2	0.52	0.04	2	0.67
R18C^{Alexa555}	1.9	4.0E-04	3.7	4.0	0.09	not obs	not obs
R18C^{PyMPO}	2	2.3E-03	3.1	4.1	0.08	1.6	5.8

Concentration dependent conformational motion associated with ligand binding was observed for all three constructs (R18C^{PyMPO}, D61C^{Alexa555} and D61C^{PyMPO} SsIGPS) by detecting changes in probe fluorescence intensity using a 550 nm filter upon excitation at 514 nm or 412 nm. In binding studies, a FRET signal resulting from energy transfer from rCdRP and IGP (ex 295 nm) to the probes generated more consistent results. The fact that concentration dependent conformational motion associated with ligand binding was observed using probe fluorescence (ex. 514 nm or 412 nm) is concordant with previous studies indicating that enzymes are flexible structures that can exist at equilibrium in different low energy conformational states. A ligand may bind to a variety of conformers with different affinity shifting the equilibrium toward enzyme-ligand complex with more favorable enzyme conformer suggesting that conformational motion increases probability of binding certain ligands (*10-12*). Structural fluctuations associated with ligand binding are well characterized, however, the field of conformational motion associated with catalysis is only now emerging as an important research area (*10, 12, 14-16*). This study demonstrates the existence of different conformational states of SsIGPS that are formed to accommodate substrate, consecutive intermediates and finally the product during the catalytic cycle of SsIGPS.

Individual microscopic rate constants for conformational motion varied among constructs labeled with different probes (Table 8) however the sequence in which they appeared was the same. The first conformational motion that follows the binding event is observed when CdRP is converted to the first intermediate and the ES complex undergoes conformational motion to form EI complex, while the second conformational motion is associated with the dehydration step and the transition from the EI2 complex to EP complex. Presence of conformational motion during course of catalysis in D61C^{Alexa555} and D61C^{PyMPO} suggests motion in the β1α1 loop (where residue 61 is located) that correlates with steps in catalysis. This motion is indirectly supported by X-ray crystallography and structural models of ES, EI, EI2 and EP complexes that suggest changes in the distance between catalytically important residue Lys53 located on the β1α1 loop

and the ligand in the binding pocket (*4*). Changes in proximity of Lys53 may determine optimum H-bond length required for consecutive steps in catalysis; therefore conformational motion in the β1α1 loop appears to be necessary for catalysis.

The role of the N-terminal extension, the α0 helix and α0α00 loop, as mentioned in the introduction, are associated primarily with binding rather than catalysis, since deletion of the first 26 amino acids affect K_M^{CdRP} but not the k_{cat} (*1*). No conformational motion, other than that associated with binding, was observed during reaction catalyzed by $R18C^{Alexa555}$. On the other hand, conformational motion associated with catalysis was observed when $R18C^{PyMPO}$ was studied, indicating that fluorescence of Alexa Fluor 555, when attached to position 18, is not sensitive enough to report on the motion of the α0α00 loop. Rate constants for the motions observed with $R18C^{PyMPO}$ are concordant with the rate constants determined for motion observed in $D61C^{Alexa555}$ and $D61C^{PyMPO}$, similarly they correlate with steps in catalysis. Since there are no catalytically important residues found on the α0α00 loop, structural rearrangements in this motif are most likely required to accommodate substrate, intermediates and the product, hence deletion of this region affects only ligand binding.

Kinetic and conformational motion studies under STO conditions were necessary to map the catalytic pathway and to better understand the complex relationship between structure and catalytic capabilities of SsIGPS. Relationship between catalysis and conformational motion in SsIGPS may provide direction for similar studies on other enzymes in the TIM-barrel family. Conformational motion in protein can correlate with steps in catalysis but the purpose of the motion may depend on the location and catalytic importance of the observed motif. It appears that motion of the loop containing catalytically important residues, like the motion in the β1α1loop in SsIGPS, is responsible for optimum proximity of functional groups, and therefore such motion may directly influence catalytic capabilities of an enzyme. The second type of motion, like the one observed with $R18C^{PyMPO}$, may be necessary to accommodate ligands and/or structural changes of the loops in near proximity. This second motion is not responsible for proper

orientation of the chemical groups, therefore it has no direct impact on the microscopic rate constants but is involved in ligand binding.

Results summarized in this thesis demonstrate for the first time presence of two distinct conformational motions each of which correlates to one particular step in catalysis. Furthermore this study provides data supporting the existence of two intermediates in the reaction catalyzed by SsIGPS. It is possible to label double SsIGPS mutants with a FRET pair and determine the magnitude of the motion as well as the direction of the motion. Future study of this sort would show explicitly the change in the arrangement of catalytically important residues. Ability to predict which functional group can be incorporated into the catalytic site would allow for more accurate and efficient drug screening and protein engineering.

6. References

1. Schneider, B.; Knochel, T.; Darimont, B.; Hennig, M.; Dietrich, S.; Babinger, K.; Kirschner, K.; Sterner, R. Role of N-terminal Extension of the $(\beta\alpha)_8$-Barrel Enzyme Indole-3-glycerol Phosphate Synthase for Its Fold, Stability, and Catalytic Activity. *Biochemistry*, **2005,** *44,* 16405-16412
2. Merz, A.; Yee, M-c.;Szadkowski, H.; Pappenberger, G,; Crameri, A.; Stemmer, W.; Yanofsky, C.; Kirschner K. Improving the Catalytic Activity of a Thermophilic Enzyme at Low Temperatures. *Biochemistry,* **2000,** *39,* 880-889.
3. Parry, R.J. Biosynthesis of Compounds Containing an Indole Nucleus. *Chem. Heterocyc. Compd.* **1972,** *25,* 1-64.
4. Hennig, M.; Darimont, B.D.; Jansonius, J.N.; Kirschner, K. The Catalytic Mechanism of Indole-3-glyceorl Phosphate Synthase: Crystal Structures of Complexes of the Enzyme from Sulfolobus solfataricus with Substrate Analogue, Substrate, and Product. *J. Mol. Biol.* **2002,** *319,* 757-766.
5. Thompson, R.B.; Maliwal, P.B.; Fierke, A.C. Selectivity and Sensitivity of Fluorescence Lifetime-Based Metal Ion Biosensing Using a Carbonic Anhydrase Transducer. *Anal. Biochem.* **1999,** *267,* 185-195.
6. Khan, F.; Gnudi, L.; Pickup, J.C. Fluorescence-based sensing of glucose using engineered glucose/galactose-binding protein: A comparison of fluorescence resonance energy transfer and environmentally sensitive dye labeling strategies. *Biochem. Bioph. Res. Co.* **2008,** *365,* 102-106.
7. Knochel, T.R.; Hennig, M.; Merz, A.; Darimont, B.; Kirschner, K.; Jansonius, J.N. The Crystal Structure of Indole-3-glycerol Phosphate Synthase from the Hyperthermophilic Archaeon *Sulfolobus solfataricus* in Three Different Crystal Forms: Effects of Ionic Strength. *J. Mol. Biol.* **1996,** *262,* 502-515.
8. Jacob, M.H.; Amir, D.; Ratner, V.; Gussakowsky, E.; Haas, E. Predicting Reactivities of Protein Surface Cysteines as Part of a Strategy for Selective Multiple Labeling. *Biochemistry.* **2005,** *44,* 13664-13672.
9. Kuzmic, P.Program DYNAFIT for the Analysis of Enzyme Kinetic Data: Application to HIV Proteinase. *Anal. Biochem.* **1996,** *237,* 260-273.
10. Vendruscolo, M.; Dobson, C.M. Dynamic Visions of Enzymatic Reactions. *Science.* **2006,** *313,* 1586-1587.
11. Xu, Y.; Nenortas, E.; Beckert, D. Evidence of Distinct Ligand-Bound Conformational States of the Multifunctional *Escherichia coli* Repressor of Biotin Biosynthesis. *Biochemistry.* **1995,** *34,* 16624-16631.
12. McElheny, D.; Schnell, J.R.; Lansing, J.C.; Dyson, H.j.; Wright, P.e. Defining the role of active loop fluctuations in dihydrofolate reductase catalysis. *P. Natl. Acad. Sci.* **2005,** *102,* 5032-5037.
13. Creighton, T.; Yanofsky, C. Indole-3-glycerol Phosphate Synthase of *Escherichia coli*, an Enzyme of the Tryptophan Operon. *J. Biol. Chem.* **1966,** *241,* 4616-4624.
14. Czekster, C.M.; Lapis, A.A.M.; Souza, G.H.M.F.; Eberlin, M.N.; Basso, L.A.; Santos, D.S.; Dupont, J.; Neto, B.A.D. The catalytic mechanism of indole-3-glycerol phosphate

synthase (IGPS) investigated by electrospray ionization (tandem) mas spectrometry. *Tetrahedron Lett.* **2008,** *49,* 5914-5917.

15. Mizoue, M.L.; Chazin, W.J. Engineering and design of ligand-induced conformational change in proteins. *Curr. Opin. Struct. Biol.* **2002,** *12,* 459-463.
16. Krajewski, W.W.; Collins, R.; Holmberg-Schiavonne, L.; Jones, T.A.; Karlberg, T.; Mowbray, S.L. Crystal Structures of Mammalian Glutamine Synthetases Illustrate Substrate-Induced Conformational Changes and Provide Opportunities for Drug and Herbicide Design. *J. Mol. Biol.* **2008,** *375,* 217-228.

7. Appendix A

Summary of fitting scripts and corresponding graphs for the IGP accumulation data (ex. 280 nm em. 320 nm cutoff filter) observed under STO conditions.

```
[task]

   data = progress
   task = fit

[mechanism]

  E + S <=====> ES      : k1    k-1
  ES <=====> EI         : k2    k-2
  EI ------> EI2        : k3
  EI2 <====> EP         : k4    k-4
  EP <===> E + P        : k5    k-5

[constants]

   k1  = 2.0
   k-1  = 0.22
   k2  = 2.7 ?
   k-2 = 0.004 ?
   k3  = 2.9 ?
   k4 = 9 ?
   k-4 = 0.06 ?
   k5 = 0.1
   k-5 = 3.47

[responses]

   E = 0.73?
   S  = 0.21 ?
   ES = 0.85?
   EI = 0.70?
   EP = 1.55?
   P =  1.4
   EI2 = 1.26 ?

[progress]

  error percent 10
  directory     ./D61C/Data
  extension     txt

  file          6E1S | concentration S = 1?, E = 6? | offset 1.28?
  file          6E2S | concentration S = 2?, E = 6? | offset 1.28?
  file          8E2S | concentration S = 2?, E = 8? | offset 1.28?
  file          8E1S | concentration S = 1?, E = 8? | offset 1.12?
  file          7E1S | concentration S = 1?, E = 7? | offset 1.28?

[output]

  directory  ./D61C/Results3final
[end]
```

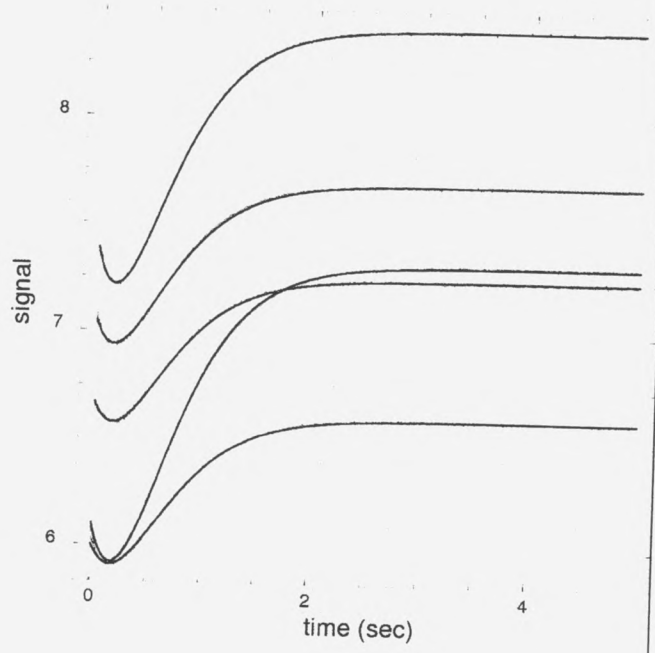

Figure I. Script used to fit IGP accumulation data determined under STO conditions for D61C^{Alexa555} in DynaFit program and the corresponding graph.

Appendix A

```
[task]

   data = progress
   task = fit

[mechanism]

  E + S <=====> ES      : k1    k-1
  ES <=====> EI         : k2    k-2
  EI ------> EI2        : k3
  EI2 <====> EP         : k4    k-4
  EP <===> E + P        : k5    k-5

[constants]

   k1  = 0.6
   k-1  = 0.019
   k2  = 1.6 ?
   k-2 = 0.013 ?
   k3  = 12 ?
   k4 = 0.54
   k-4 = 0.005 ?
   k5 = 0.038
   k-5 = 1.36

[responses]

   E = 0.62  ?
   S  = 0.17 ?
   ES = 0.7 ?
   EI = 0.45
   EP = 1.8?
   P = 1.60
   EI2 = 1.62 ?

[progress]

  error percent 10
  directory     ./D61Cpympo/Data
  extension     txt

   file         6E1S | concentration S = 1? , E = 6? | offset   0.72?
   file         6E2S | concentration S = 2? , E = 6? | offset   0.9 ?
   file         8E2S | concentration S = 2? , E = 8? | offset   0.7 ?
   file         8E1S | concentration S = 1? , E = 8? | offset   1.1 ?
   file         7E1S | concentration S = 1? , E = 7? | offset   1.1 ?

[output]

  directory  ./D61Cpympo/Resultsfinal
[end]
```

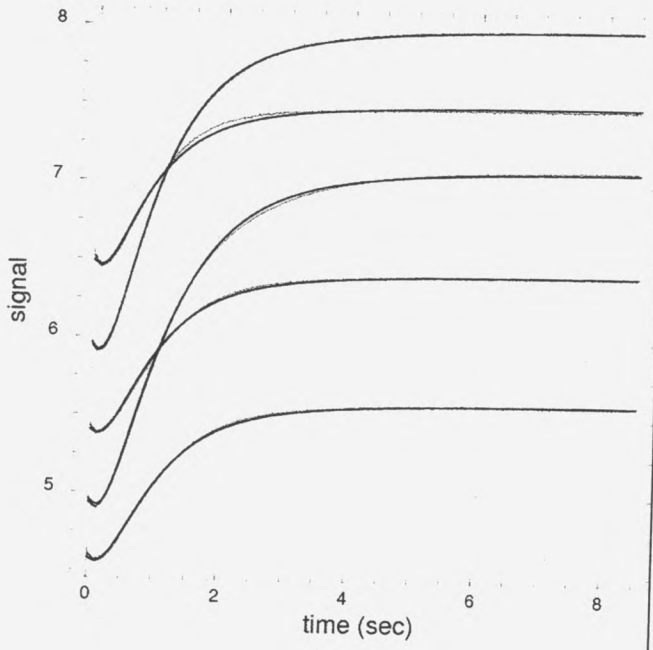

Figure II. Script used to fit IGP accumulation data determined under STO conditions for D61C^{PyMPO} in DynaFit program and the corresponding graph.

Appendix A

```
[task]

   data = progress
   task = fit

[mechanism]

  E + S <=====> ES      : k1    k-1
  ES <=====> EI         : k2    k-2
  EI ------> EI2        : k3
  EI2 <====> EP         : k4    k-4
  EP <===> E + P        : k5    k-5

[constants]

   k1  = 3.7
   k-1  = 0.32
   k2  = 1.9  ?
   k-2 = 0.013 ?
   k3  = 3.4 ?
   k4 = 4.6  ?
   k-4 = 0.017 ?
   k5 = 0.04
   k-5 = 5.5

[responses]

   E = 0.88 ?
   S  = 0.26 ?
   ES = 1.01 ?
   EI = 0.46 ?
   EP = 1.81 ?
   P =  1.8
   EI2 = 1.2 ?

[progress]

  error percent 10
  directory     ./R18Calexa/Data
  extension     txt

  file          6E1S | concentration S = 1? , E = 6? | offset   0.6 ?
  file          6E2S | concentration S = 2? , E = 6? | offset   0.6 ?
  file          8E2S | concentration S = 2? , E = 8? | offset   0.6 ?
  file          8E1S | concentration S = 1? , E = 8? | offset   0.6 ?
  file          7E1S | concentration S = 1? , E = 7? | offset   0.6 ?

[output]

  directory  ./R18Calexa/Resultsfinal
[end]
```

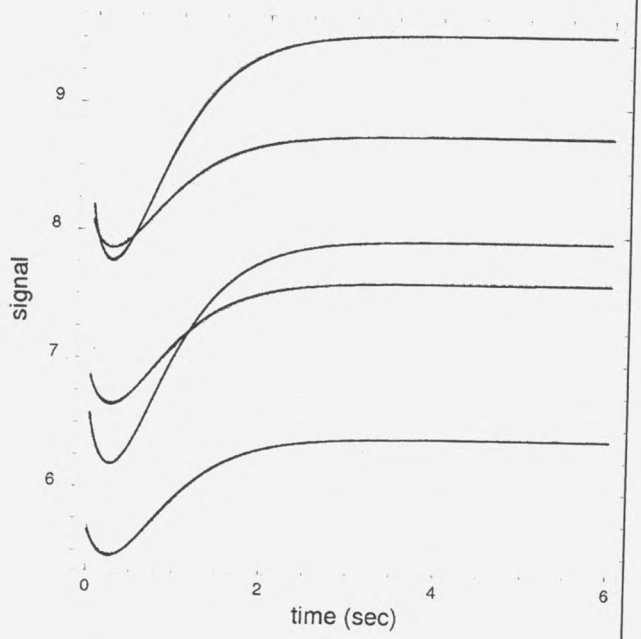

Figure III. Script used to fit IGP accumulation data determined under STO conditions for R18C^{Alexa555} in DynaFit program and the corresponding graph.

Appendix A

```
[task]

   data = progress
   task = fit

[mechanism]

  E + S <=====> ES      : k1    k-1
  ES <=====> EI         : k2    k-2
  EI ------> EI2        : k3
  EI2 <====> EP         : k4    k-4
  EP <===> E + P        : k5    k-5

[constants]

   k1  = 3.45
   k-1  = 0.31
   k2  = 2.0 ?
   k-2 = 0.002 ?
   k3  = 3.1 ?
   k4 = 4.5 ?
   k-4 = 0.002 ?
   k5 = 0.04 ?
   k-5 = 5.5

[responses]

   E = 0.89 ?
   S  = 0.12 ?
   ES = 1.02 ?
   EI = 0.6 ?
   EP = 1.47  ?
   P =  1.2
   EI2 = 1.2 ?

[progress]

  error percent 10
  directory      ./R18Cpympo/Data
  extension      txt

  file           6E1S | concentration S = 1?, E = 6? | offset 0.3?
  file           6E2S | concentration S = 2?, E = 6? | offset 0.3?
  file           8E2S | concentration S = 2?, E = 8? | offset 0.3?
  file           8E1S | concentration S = 1?, E = 8? | offset 0.3?
  file           7E1S | concentration S = 1?, E = 7? | offset 0.3?

[output]

  directory  ./R18Cpympo/Results3b
[end]
```

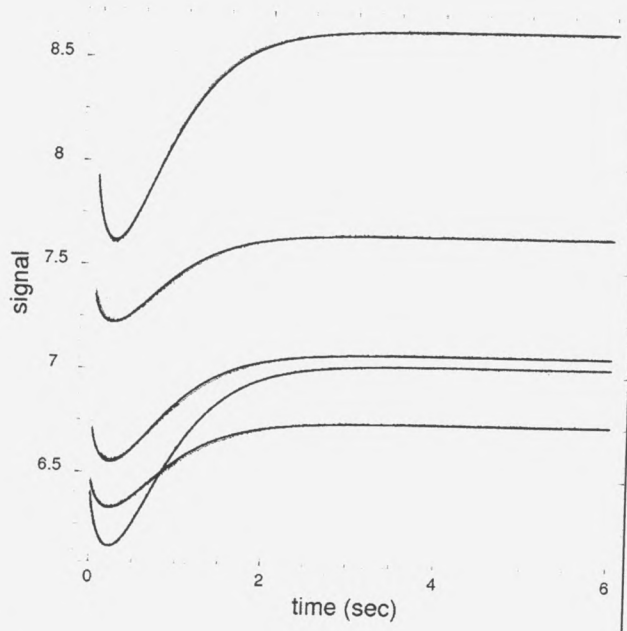

Figure IV. Script used to fit IGP accumulation data determined under STO conditions for R18C^{PyMPO} in DynaFit program and the corresponding graph.

8. Appendix B

Summary of fitting scripts and corresponding graphs for conformational motion associated with catalysis of CdRP (ex. 514 nm Alexa 555, ex. 412 nm PyMPO, em. 550 nm cutoff filter both probes) observed under STO conditions.

```
[task]

  data = progress
  task = fit

[mechanism]

 E -----> E'          : k2'
 E' -----> E''        : k4'

[constants]

  k2' = 2.9 ?
  k4' = 9.2 ?

[responses]

  ;E = 1.03?
  ;E' = 1.0 ?
  ;E'' = 1.05?

[progress]

 error percent 10
 directory    ./D61CAlexa514/Data
 extension    txt
 ;offset      0.3 ? local

file   6E1S | concentration E = 6 | offset 0? | response E = 1.03? | response E'  = 1.0? | response E'' = 1.05?

file   6E2S | concentration E = 6 | offset 0? |response E = 1.03? | response E'  = 1.0? | response E'' = 1.05?

file   8E2S | concentration E = 8 | offset 0?| response E = 1.03? | response E'  = 1.0? | response E'' = 1.05?

file   8E1S | concentration E = 8 | offset 0? | response E = 1.03? | response E'  = 1.0? | response E'' = 1.05?

file   7E1S | concentration E = 7 | offset 0? | response E = 1.03? | response E'  = 1.0? | response E'' = 1.05?

[output]

 directory ./D61CAlexa514/Results

[end]
```

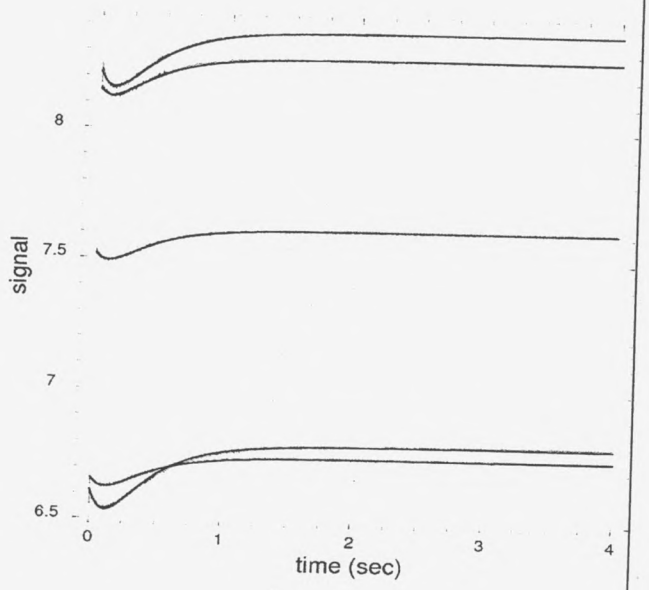

Figure V. Script used to fit conformational motion data determined under STO conditions for D61C^{Alexa555} in DynaFit program and the corresponding graph.

Appendix B

```
[task]

   data = progress
   task = fit

[mechanism]

  E  -----> E'          : k2'
  E' -----> E''         : k4'

[constants]

   k2' = 2.0 ?
   k4' = 0.7 ?

[responses]

   ;E = 0.86 ?
   ;E' = 1.1 ?
   ;E'' = 1?

[progress]

  error percent 10
  directory    ./D61CPympo412/Data
  extension    txt
  ;offset      0.3 ? local

file   6E1S | concentration E = 6 | offset 0? | response E = 0.82? | response E' = 0.88 ? | response E'' = 0.94 ?

file   6E2S | concentration E = 6 | offset 0?  | response E = 0.82? | response E' = 0.88 ? | response E'' = 0.94 ?
file   8E2S | concentration E = 8 | offset 0?  | response E = 0.82? | response E' = 0.88 ? | response E'' = 0.94 ?
file   8E1S | concentration E = 8 | offset 0?  | response E = 0.82? | response E' = 0.88 ? | response E'' = 0.94 ?

file   7E1S | concentration E = 7 | offset 0  | response E = 0.82? | response E' = 0.88 ? | response E'' = 0.94 ?

[output]

  directory  ./D61CPympo412/Results

[end]
```

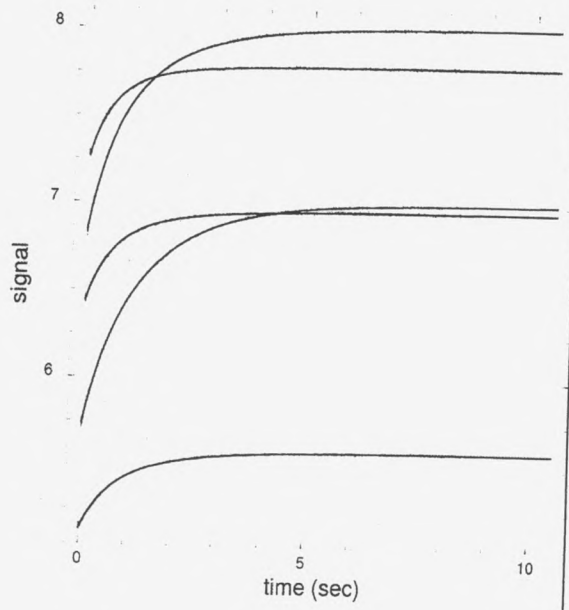

Figure VI. Script used to fit conformational motion data determined under STO conditions for D61C^{PyMPO} in DynaFit program and the corresponding graph.

Appendix B

```
[task]

  data = progress
  task = fit

[mechanism]

 E -----> E'          : k2'
 E' -----> E''        : k4'

[constants]

  k2'  = 5.7 ?
  k4' = 9.2 ?

[responses]

  ;E = 1.03?
  ;E' = 1.0 ?
  ;E'' = 1.05?

[progress]

 error percent 10
 directory    ./R18Calexa514/Data
 extension    txt

file   6E1Scorrected | concentration E = 6 | offset -6? | response E = 1.03? | response E'  = 1.0? | response E'' = 0.95?

file   6E2Scorrected | concentration E = 6 | offset -6? | response E = 1.03? | response E'  = 1.0? | response E'' = 0.95?

file   8E2Scorrected | concentration E = 8 | offset -8?| response E = 1.03? | response E'  = 1.0? | response E'' = 0.95?

file   8E1Scorrected | concentration E = 8 | offset -8? | response E = 1.03? | response E'  = 1.0? | response E'' = 0.95?

file   7E1Scorrected | concentration E = 7 | offset -7? |response E = 1.03? | response E'  = 1.0? | response E'' = 0.95?

[output]

 directory  ./R18Calexa514/Results2

[end]
```

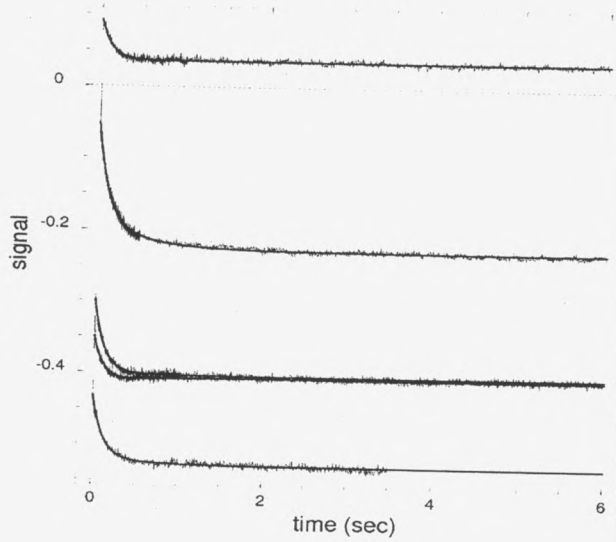

Figure VII. Script used to fit conformational motion data determined under STO conditions for $R18C^{Alexa555}$ in DynaFit program and the corresponding graph.

Appendix B

```
[task]

  data = progress
  task = fit

[mechanism]

 E  -----> E'          : k2'
 E' -----> E''         : k4'

[constants]

  k2'  = 2.1 ?
  k4' = 5.7 ?

[responses]

  ;E = 1.03?
  ;E' = 1.0 ?
  ;E'' = 1.05?

[progress]

 error percent 10
 directory     ./R18Cpympo412/Data
 extension     txt
 ;offset       0.3 ? local

file   6E1S | concentration E = 6 | offset 0?| response E = 1.05? | response E'  = 1.0? | response E'' = 1.07?

file   6E2S | concentration E = 6 | offset 0?| response E = 1.05? | response E'  = 1.0? | response E'' = 1.07?

file   8E2S | concentration E = 8 | offset 0?| response E = 1.05? | response E'  = 1.0? | response E'' = 1.07?

file   8E1S | concentration E = 8 | offset 0?| response E = 1.05? | response E'  = 1.0? | response E'' = 1.07?

file   7E1S | concentration E = 7 | offset 0?| response E = 1.05? | response E'  = 1.0? | response E'' = 1.07?

[output]

 directory  ./R18Cpympo412/Results

[end]
```

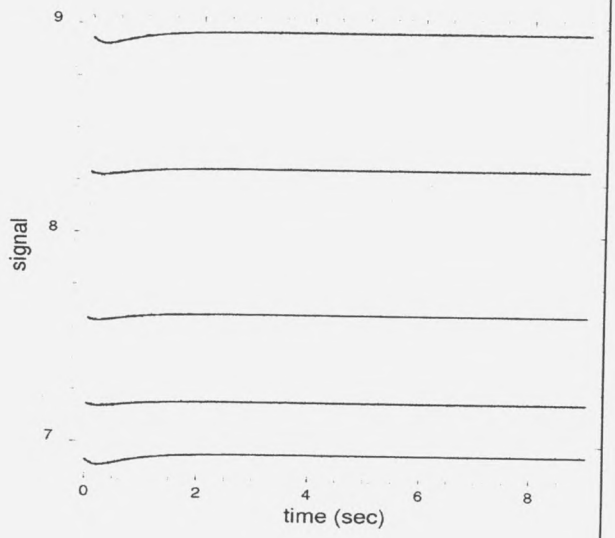

Figure VIII. Script used to fit conformational motion data determined under STO conditions for R18C^{PyMPO} in DynaFit program and the corresponding graph.

9. Appendix C

Summary of fitting scripts and corresponding graphs for the conformational motion (ex. 514 nm em. 550 nm cutoff filter) observed under MTO conditions.

```
[task]

   data = progress
   task = fit

[mechanism]

  E -----> E'        : k2'
  E' -----> E''      : k4'


[constants]

   k2' = 3?
   k4' = 10?

[progress]

  error percent 10
  directory     ./D61CAlexa514/DataMTO/Data
  extension     txt
  ;offset       0.3 ? local

file   1E10S | concentration E = 1 | offset -8.4? | response E = 15.7? | response E'  = 14.6? | response E'' = 16.2?

file   1E20S | concentration E = 1 | offset -8.4? | response E = 15.7? | response E'  = 14.6? | response E'' = 16.2?

file   1E30S | concentration E = 1 | offset -8.4? | response E = 15.7? | response E'  = 14.6? | response E'' = 16.2?

file   05E5S | concentration E = 0.5 | offset -10 ? | response E = 17? | response E'  = 14? | response E'' = 18?


[output]

  directory  ./D61CAlexa514/DataMTO/Results

[end]
```

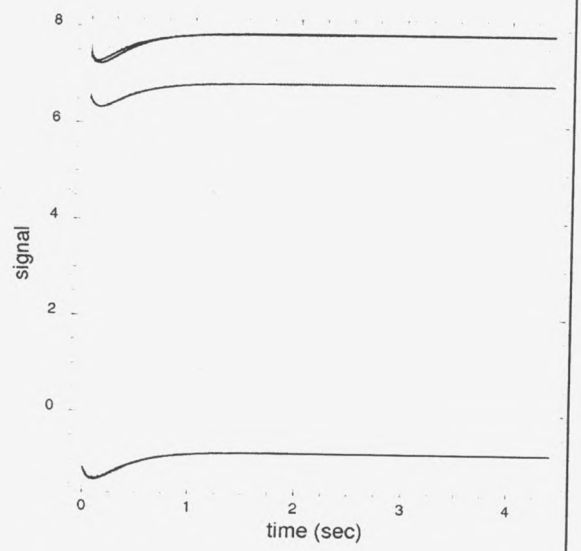

Figure IX. Script used to fit conformational motion data determined under MTO conditions for $D61C^{Alexa555}$ in DynaFit program and the corresponding graph.